https://doi.org/10.5194/egusphere-2026-3721
Preprint. Discussion started: 22 July 2026

ATDT v1.0 - Attribution Tool for Daily-to-monthly Temperatures and its application to record-breaking Northern European heatwave of July 2025

Antti Toropainen[1], Mika Rantanen[2], and Jouni Räisänen[1]

[1]University of Helsinki, Institute for Atmospheric and Earth System Research/Physics, Faculty of Science, P.O. Box 64, Helsinki, 00140, Finland
[2]Finnish Meteorological Institute, Erik Palménin aukio 1, Helsinki, 00560, Finland

Correspondence: Antti Toropainen (antti.toropainen@helsinki.fi)

Abstract. We present here ATDT (Attribution Tool for Daily-to-monthly Temperatures), a method for quantifying the effect of climate change on local daily mean, maximum and minimum temperatures as well as their 2–31-day moving averages for locations that have long observational time-series available. The method utilizes CMIP6 (Coupled Model Intercomparison Project Phase 6) model data and a time series of global mean temperature to estimate climate-change-induced shifts in both the mean and variance of local temperature distributions. As a case study, we apply the method to 23 weather stations in Fennoscandia for two 14-day periods in July of 2025, when an intense heatwave occurred in Northern Europe. We find that the station-specific average maximum temperatures in 12-25 July were 1.5 to 2.4 °C higher, whereas the minimum temperatures in 19 July to 1 August were 1.4 to 2.3 °C higher than they would have been under pre-industrial conditions represented by the year 1900. Furthermore, we estimate that these temperatures were made 3.0–14.6 times (maximum temperature) and 6.1–22.9 times (minimum temperature) more likely by climate change since the year 1900. The presented method enables real-time attribution of climate change on observed temperatures and can support operational meteorologists in climate change communication.

1 Introduction

The ongoing climate change is manifested not only in rising mean temperatures but also in an increasing number of extreme weather events, such as heatwaves and heavy rainfall (Fischer and Knutti, 2015; Donat et al., 2013; Perkins et al., 2012; Rahmstorf and Coumou, 2011). Extreme weather events, which often have the largest societal and economic impacts, are also viewed by the general public as evidence of anthropogenic climate change. Consequently, in the aftermath of a high-impact weather event, meteorologists and climate scientists are frequently asked by the media and general public if the event was affected by climate change. In the past, this kind of a question has been been answered typically, for example, by comparing the return periods of similar events from two different 30-year climatological periods. Such an approach only yields a rough estimate on changes in probability of occurrence without providing accurate information on how climate change affected the frequency and intensity of the event itself, which would be essential for both developing adaptation strategies (Zhang et al., 2024) and

https://doi.org/10.5194/egusphere-2026-3721
Preprint. Discussion started: 22 July 2026

educating the general public (Maibach et al., 2022).

Extreme weather attribution has progressed considerably over the past decade or so, becoming a subfield of climate science (Otto, 2017; van Oldenborgh et al., 2021; Nature Climate Change, 2024) and is increasingly approaching operational level (Gilford et al., 2022; Otto et al., 2022; Stott and Christidis, 2023). Over the recent years, several high-impact weather events have been attributed to climate change (Seneviratne et al., 2021; Philip et al., 2022; Athanase et al., 2024; Leach et al., 2024; Calvo-Sancho et al., 2026). One of the leading organizations conducting these studies is the World Weather Attribution (WWA) which, in addition to having developed an attribution methodology (Philip et al., 2020), has performed over 100 attribution studies of globally high-impact weather events, including heatwaves, heavy rainfall, droughts, floods, wildfires and cold spells (World Weather Attribution, 2026). However, smaller-scale extreme events, impacting nations, counties and municipalities may also be of high societal interest, underscoring the need for additional national attribution services.

In the Nordic countries, and particularly in Finland, attribution research has recently advanced from methodological development towards operational level. A probabilistic attribution method has been developed to quantify the influence of climate change on monthly, seasonal, and annual temperatures (Rantanen et al., 2024). The method has subsequently been adopted operationally by the Finnish Meteorological Institute and is regularly used in monthly climate summaries and media communications following anomalously warm months and seasons (FMI, 2026). One example was the exceptionally warm summer of 2024 in northern Fennoscandia, which was estimated to have been approximately 2.1°C warmer and about 100 times more likely because of climate warming since 1900 (Rantanen et al., 2025). Outside of Finland, the method has been applied also for eastern Europe's hot summer 2024 (Ionita and Nagavciuc, 2025) and Norway's record-warm year 2025 (Skålevåg, 2026).

Many high-impact temperature extremes, however, occur on timescales shorter than one month or span two calendar months. As a result, the attribution method from Rantanen et al. (2024) that is based on monthly mean temperatures does not adequately characterize the magnitude or probability of such events. Furthermore, the most relevant temperature metric depends on the nature of the event. For heatwaves, daily maximum temperatures are often of primary interest, whereas cold spells may be better characterized by daily minimum temperatures. In some situations, daily mean temperature may provide the most representative measure of the event. Likewise, the timescale of interest can range from a single day to a multi-day period corresponding to the duration of the event. An operational attribution tool should therefore be sufficiently flexible to accommodate different temperature variables and event durations.

In this paper, we present the ATDT attribution tool, which quantifies the effect of climate change on observed daily mean, maximum and minimum temperatures or their 2 to 31-day moving averages. The tool enables meteorologists and climate scientists to report in near-real-time the impact of climate change on ongoing or just observed temperature extremes, for example, to media and general public. The described method is based on CMIP6 data, time-series of global mean temperature

https://doi.org/10.5194/egusphere-2026-3721
Preprint. Discussion started: 22 July 2026

and local daily mean, maximum and minimum temperature observations. As a case study, we apply the method to a heatwave which occurred in Northern Europe in July 2025.

2 Data and methods

In 2008, Räisänen and Ruokolainen (2008a) proposed a model-based method for estimating the actual present-day temperature climate in a warming world. The method proved to be more successful in predicting the observed temperature climate over land areas during 1991-2002 than the more conventional way of predicting the climate from past observations alone and it was subsequently used to quantify the effect of climate change on the extremely mild temperatures of December 2006 and March 2007 in Finland (Räisänen and Ruokolainen, 2008b). In 2023, the method was modified and extended by Rantanen et al. (2024) (hereafter denoted as the RRR-method) so that meteorologists and climatologists can use it operationally for attributing extreme monthly and seasonal temperatures to climate change. Its capability to estimate the probability distributions of monthly temperature has been verified by Räisänen et al. (2025), using both station observations and European Centre for Medium-Range Weather Forecasts ERA5 reanalysis Hersbach et al. (2020) data. They demonstrated its ability to provide nearly statistically reliable probability estimates in a changing climate without using any observations that would not have been available in an operational setting.

Here, we extend the RRR-method further for the purpose of estimating the effect of climate change on the observed daily mean, maximum and minimum temperatures as well as their 2 to 31-day moving averages. To accomplish this, we have modified the methods to estimate changes in the local mean and variability, and to fit a continuous probability distribution. The method for estimating uncertainty of the attribution results has also been revised. A brief summary of the used data and the main steps of the method are also shown in Figure 1. The following sub-sections describe the used data and each step of the methodology in detail.

2.1 Observational data

The presented method uses in-situ daily mean, maximum and minimum 2-meter temperature observations from the weather stations of Finnish Meteorological Institute (FMI), Swedish Hydrological and Meteorological Institute (SMHI) and MetNorway (METNO) (the top left box in Figure 1). While we only use observations from Fennoscandia in this study, the proposed method should, in principle, work for any local daily temperature observations, provided that the observational time series is sufficiently long. In the context of extreme weather event attribution, the time-series that includes the event should go back at least 50 and preferably more than 100 years (van Oldenborgh et al., 2021). As a compromise, we will use observational time-series which are at least 70 years long in this study, due to the small number of Fennoscandian stations that have a 100-year long time-series of daily observations readily available. A list of used weather-stations is shown in Table A1. In addition to local observations, the method uses the observed annual global mean temperature time-series (the top center box in Figure

https://doi.org/10.5194/egusphere-2026-3721
Preprint. Discussion started: 22 July 2026

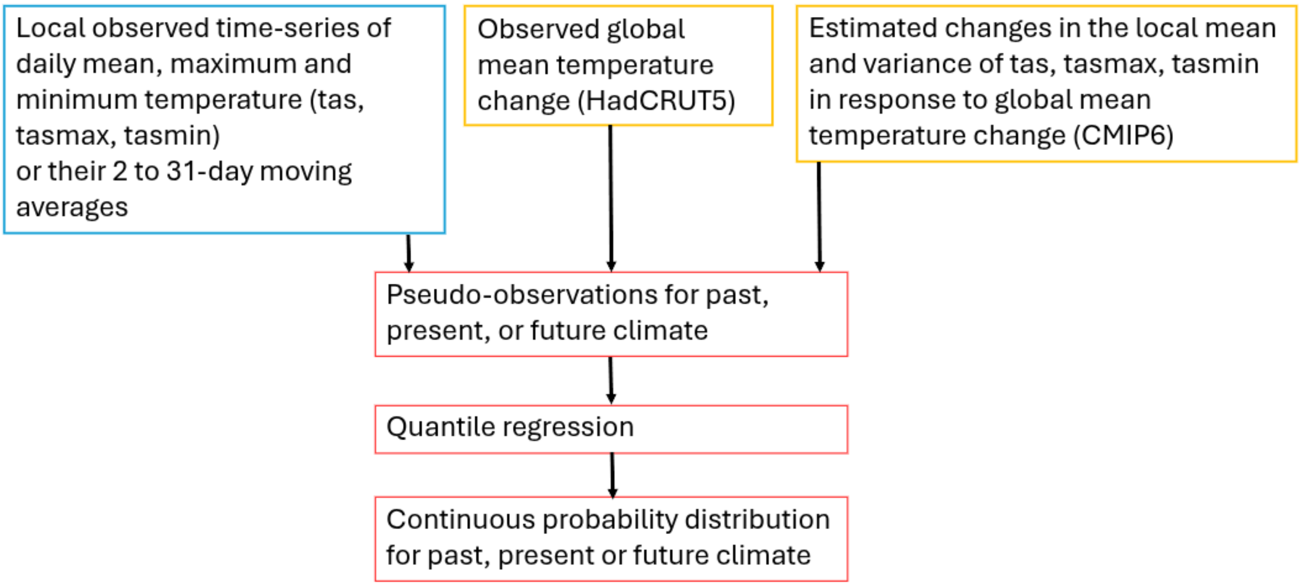

Figure 1. Flowchart illustrating the methodology. The three boxes at the top describe the used data while the red boxes below them show the main steps of the methodology.

1) as provided by Met Office Hadley Centre/Climatic Research Unit global surface temperature data set HadCRUT5 (Morice et al., 2021).

2.2 Model data

The method also uses data from 31 coupled climate models in the Coupled Model Intercomparison Project Phase 6 (CMIP6 Eyring et al. (2016)). For each model, we extract the near-surface air temperature variables: daily mean (variable "tas"), daily minimum ("tasmin"), and daily maximum ("tasmax"). The simulations cover both historical (1900–2014) and future (2015–2100) periods, with future projections provided by five different Shared Socio-economic Pathway (SSP) scenarios. For each model and variable, we concatenate the historical and scenario simulations to form a continuous time series of global mean temperature for 1900–2100. The CMIP6-data is used to estimate the future time-evolution of global mean temperature, which depends on the projected increase of greenhouse gas emissions, and the change in local climate in response to global temperature increase. In the context of attributing extreme temperatures, the chosen scenario has a major impact only in the future climate. A list of used models is shown in Table S1.

https://doi.org/10.5194/egusphere-2026-3721
Preprint. Discussion started: 22 July 2026

3 Methods

3.1 Regression equations

By using CMIP6-data, we estimate how the local climate changes in response to the global mean temperature change (the top right box in Figure 1). Let $x_\mathrm{n}(d,t)$ denote the n-day average of daily mean, maximum or minimum 2-meter temperature where d is the corresponding day-of-year index. When n is odd, d is the central day-of-year of the period. When n is even, it is the latter of the two central days. For example, for the period 1-3rd January, $n = 3$ and $d = 2$. For 1-4th January, $n = 4$ and $d = 3$.

The local time-dependent weather parameter $x_\mathrm{n}(d,t)$ can be written as a sum of $\overline{x_\mathrm{n}}(d,t)$ and $x'_\mathrm{n}(d,t)$, where the former represents the time-dependent expected value of $x_\mathrm{n}(d,t)$ and the latter a deviation from it due to internal climate variability:

$$x_\mathrm{n}(d,t) = \overline{x_\mathrm{n}}(d,t) + x'_\mathrm{n}(d,t) \tag{1}$$

Next, we assume that the expected value $\overline{x_\mathrm{n}}(d,t)$ (eq. 2) and the expected square of its deviation $\overline{x'_\mathrm{n}}(d,t)^2$, representing the expected value of inter-annual variance (eq. 3) depend linearly on the low-pass-filtered (11-year running mean) global mean temperature $G_{11}(t)$. The justifications for these assumptions and the choice of averaging the global mean temperature over the somewhat arbitrary 11-year period are discussed in Räisänen and Ruokolainen (2008a) and Rantanen et al. (2024).

$$\overline{x_\mathrm{n}}(d,t) = A_\mathrm{n}(d) + B_\mathrm{n}(d) \cdot G_{11}(t) \tag{2}$$

$$\overline{x'_\mathrm{n}}(d,t)^2 = C_\mathrm{n}(d) + D_\mathrm{n}(d) \cdot G_{11}(t) \tag{3}$$

The coefficients in Eqs. 2 and 3 are determined by ordinary least-square (OLS) linear regression. OLS is first applied to Eq. 2 and then to Eq. 3 by regressing the square of the residual from Eq. 2. Finally, $D_\mathrm{n}(d)$ is converted to relative units by dividing it with the inter-annual variance of year 2000 (Rantanen et al., 2024).

The regression coefficients in Eqs. 2 and 3 are calculated separately for each CMIP6 model by using the simulated time-series of local daily mean, maximum and minimum near-surface air temperature. In addition to daily values, regression is also applied to 3-, 7-, 15- and 31-day moving averages of the three temperature parameters. Thus, for all n-day averages, the total number of regression coefficients over a calendar year equals the number of days in the model's calendar.

The simulated time-series of daily local temperature and other weather variables are subject to internal variability arising from the chaotic dynamics of the climate system (Lorenz, 1963). Consequently, the calculated model-specific regression coefficients B_n and D_n also contain stochastic variability that has no predictive value. This is evident in Figure 2 which shows that the seasonal evolution of B_1 and D_1 of daily near-surface air temperature at the grid point of Helsinki, Finland includes both short-term (sub-monthly) internal variability and longer-term quasi-periodic seasonal variability. The model-specific regression coefficients could be, in principle, estimated more precisely by running a large ensemble of simulations with slightly varying initial conditions. However, such ensembles are not available for all models used in this study and the computational

https://doi.org/10.5194/egusphere-2026-3721
Preprint. Discussion started: 22 July 2026

cost of estimating the coefficients for all model realizations would be very high. Therefore, we will only use one realization of the climate per climate model in calculating the regression coefficients.

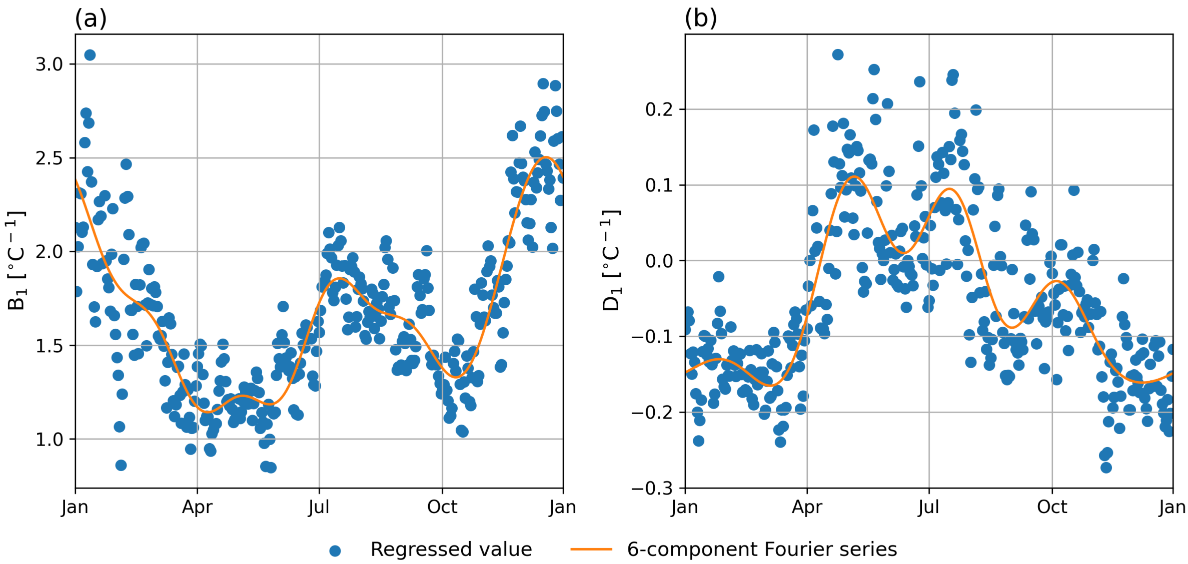

Figure 2. The daily values of regression coefficients B_1 (a) and D_1 (b) from Eqs. 2 and 3 for the daily mean near-surface temperature and their corresponding 6-component Fourier-series at the grid point nearest to Helsinki, Finland (60.2 °N, 24.9 °E), based on data from the ACCESS-CM2 model under the SSP2-4.5 scenario.

To reduce the internal short-term variability while capturing the quasi-periodic seasonal variability, a 6-component Fourier series is fitted by OLS-regression to both the seasonal evolution of B_n and D_n for each n-day mean over the model's calendar year. Figure 2 shows that fitting a Fourier-series effectively smooths most of the observed variability in the sub-monthly scale and retains the model-specific variation in seasonal time-scale. The fitted Fourier-series of models that have a 360-day calendar (models HadGEM3-GC31-LL, KACE-1-0-G, UKESM1-0-LL) have been interpolated to a 365-day calendar.

The resulting regression coefficients vary between models due to inter-model differences in how global warming is distributed across regions, as well as residual effects of internal variability. In the multi-model mean coefficients, hereafter denoted $\langle B_\mathrm{n}(d)\rangle$ and $\langle D_\mathrm{n}(d)\rangle$, respectively, the effects of internal variability and unsystematic model errors are substantially reduced. All the regression coefficients are first calculated in each model's original grid, after which they are interpolated to a common 2.5° × 2.5° latitude-longitude grid.

Figure 3 shows the multi-model mean regression coefficients for the daily mean temperature and its 3-, 7-, 15- and 31-day averages at the grid point nearest to Helsinki, Finland. The expected mean temperature ($\langle B_\mathrm{n}\rangle$) is projected to increase 1.4 to

https://doi.org/10.5194/egusphere-2026-3721
Preprint. Discussion started: 22 July 2026

2.2 °C for every 1 °C of global warming independent of the length of the time-scale, with the greatest warming occurring in winter months and the lowest in early summer and mid-autumn. The observed seasonal trend of $\langle B_{\mathrm{n}} \rangle$ qualitatively agrees with the observed warming in Finland with some differences in the details (Mikkonen et al., 2015; Räisänen, 2019; Ruosteenoja and Räisänen, 2021). Inter-annual variance ($\langle D_{\mathrm{n}} \rangle$) is projected to decrease the most during winter months (15 to 22 % for 1 °C of global warming), whereas a small 1 to 6 % increase is projected to occur during summer months. In contrast to the expected value ($\langle B_{\mathrm{n}} \rangle$, Fig. 3), the length of the time-scale affects to some extent the projected change in variability. This is why we have calculated regression coefficients more (less) frequently at short (long) time-scales. For periods other than 1, 3, 7, 15 and 31 days, regression coefficients are obtained by linear interpolation.

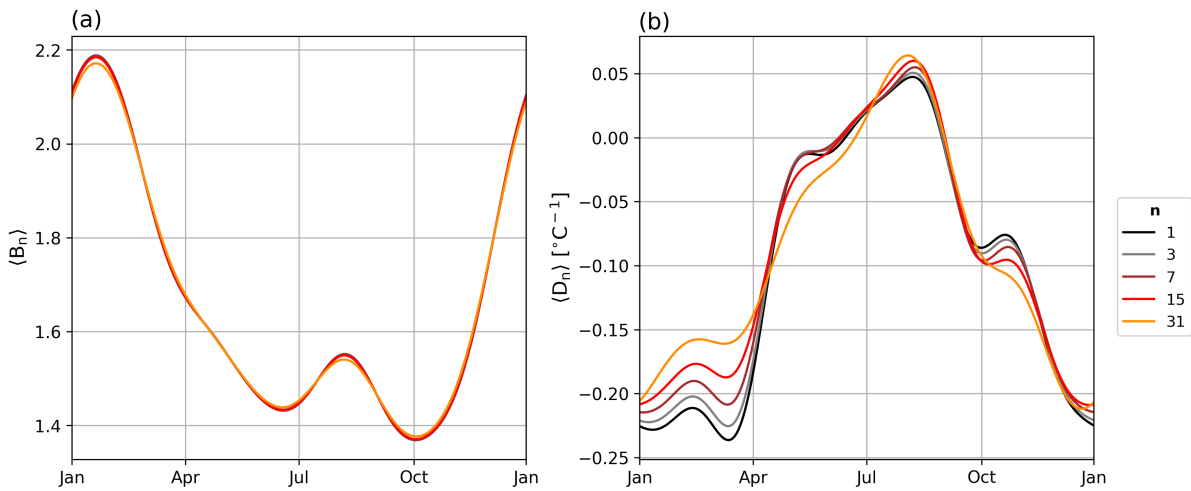

Figure 3. The seasonal variation of multi-model mean regression coefficients (a) $\langle B_{\mathrm{n}} \rangle$ and (b) $\langle D_{\mathrm{n}} \rangle$ for 1, 3, 7, 15 and 31-day mean temperatures, according to Hist+SSP2-4.5 scenario (See Table S1) at the grid point nearest to Helsinki, Finland.

3.2 Derivation of pseudo-observations

The first step in the presented method is to convert the in-situ temperature observations to climate change adjusted pseudo-observations which represent a stationary past, present-day or future climate (upper red box in Figure 1). Pseudo-observations can be derived according to the equations presented in Räisänen and Ruokolainen (2008a) and Rantanen et al. (2024) both by using the multi-model mean coefficients $\langle B_{\mathrm{n}} \rangle$ and $\langle D_{\mathrm{n}} \rangle$ and the the model-specific coefficients B_{n} and D_{n}. The best-estimate results provided by the method are based on the former, whereas the latter are needed in deriving the uncertainty estimates. For demonstrative purposes, we will use the multi-model mean coefficients in the following (Eqs. 4–7).

Let $x_{\mathrm{n}}(t_0)_{\mathrm{obs}}$ denote the observed n-day mean of mean, maximum or minimum temperature in the year t_0. The climate-change adjusted pseudo-observation $y_{\mathrm{n}}(t_0,t)_{\mathrm{obs}}$, representing the "analogy" of the observed value in a stationary climate in the year t

https://doi.org/10.5194/egusphere-2026-3721
Preprint. Discussion started: 22 July 2026

is derived in two steps. First, we estimate the impact of change in the mean climate as follows:

$$z_n(t_0,t)_{\mathrm{obs}} = x_n(t_0)_{\mathrm{obs}} + \langle B_{\mathrm{n}} \rangle \cdot \Delta G_{11}(t_0,t) \tag{4}$$

where $\Delta G_{11}(t_0,t)$ is the change in the 11-year running mean of global mean temperature G_{11} between t_0 and t. The change in $G_{11}(t)$ is derived by concatenating the observed time-series of G_{11} from t_0 to t_{ref} with the simulated time-series G_{11} from t_{ref} to t:

$$\Delta G_{11}(t_0,t) = \Delta G_{11}(t_0,t_{\mathrm{ref}})_{\mathrm{obs}} + \Delta G_{11}(t_{\mathrm{ref}},t)_{\mathrm{sim}} \tag{5}$$

Currently, t_{ref} = 2020, as G_{11} observations are available up to that year. The final pseudo-observations $y_{\mathrm{n}}(t)_{\mathrm{obs}}$ are obtained by accounting for the change in variability:

$$y_{\mathrm{n}}(t)_{\mathrm{obs}} = Z_{\mathrm{n}}(t) + \sqrt{R_{\mathrm{n}}(t_0,t)}\big(z_{\mathrm{n}}(t_0,t)_{\mathrm{obs}} - Z_{\mathrm{n}}(t)\big) \tag{6}$$

where $Z_{\mathrm{n}}(t)$ is the average of $z_{\mathrm{n}}(t)_{\mathrm{obs}}$ over the entire baseline period (1901-2024 or from the first year of observation to the year 2024 if the time-series starts later than 1901) and $R_{\mathrm{n}}(t_0,t)$ signifies the ratio of variance between times t and t_0:

$$R_{\mathrm{n}}(t_0,t) = \frac{\overline{x'_{\mathrm{n}}(t)^2}}{\overline{x'_{\mathrm{n}}(t)^2} - \langle D_{\mathrm{n}} \rangle \cdot G_{11}(t_0,t)} \tag{7}$$

Eqs. 4-7 convert temperature observations to pseudo-observations which represent the analogy of the observed time-series in the climate of year t. In this study, pseudo-observations are calculated for the years 1900, 2025 and 2050. The year 1900 approximates the pre-industrial climate while the years 2025 and 2050 represent the present-day and future climate.

Figure 4 shows the observed time-series of 14-day moving average of daily maximum temperature in Sodankylä, Finland over the time period of 12-25 July in the years 1908-2025. The observed temperature of 28.0 °C in 2025 was the second highest such period in the station's history, only falling below the record hot heatwave in the summer of 2018. However, pseudo-observations suggest that the heat wave which occurred in 1938 would have been nearly 2 °C warmer in the present-day climate and had approximately the same intensity as the heat wave of 2025.

3.3 Quantile regression

The second step in the presented attribution method is to perform quantile regression (QR) to pseudo-observations, representing pre-industrial, present-day and future climates, for the purpose of converting them to continuous probability distributions (the center red box in Figure 1). This includes two steps. First, QR is used to estimate the seasonal evolution of quantiles by using 6 Fourier components as predictors, in order to reduce the random noise in the original daily observations. Second, an analytical probability distribution is fitted to the quantiles which correspond to the selected time-period (e.g. 12-25 July).

QR is a statistical framework which extends the ordinary least-square estimation of the conditional mean function to the estimation of conditional quantiles functions (Koenker and Bassett, 1978; Koenker and Hallock, 2001). Although originally

https://doi.org/10.5194/egusphere-2026-3721
Preprint. Discussion started: 22 July 2026

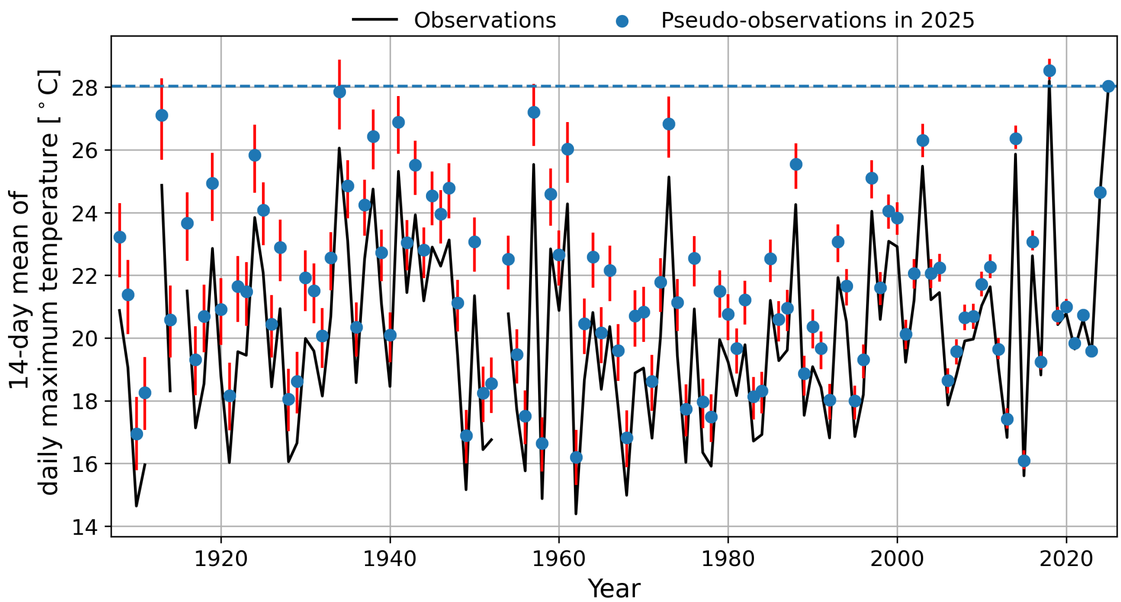

Figure 4. Time-series of the observed 14-day average daily maximum temperature for the period Jul 12th - Jul 25th in Sodankylä, Finland (67.4 °N, 26.6 °E). Black line shows the actual observation, blue dots show the corresponding multi-model mean pseudo-observations, representing present-day climate. The red error bars show the 5th and 95th percentiles of the ensemble of 29 model-specific pseudo-observations. The blue dashed line marks the observation (28.0 °C) of year 2025.

developed for econometrics, quantile regression has been applied in several geo-scientific contexts to the study of, for example, temperature, precipitation and sea level height observations (Barbosa, 2008; Barbosa et al., 2011; Wasko and Sharma, 2014; Gao and Franzke, 2017; Haugen et al., 2018; Poppick and McKinnon, 2020; Duan et al., 2022).

In this study, quantile regression is performed to all quantiles $\tau = \{0.01...0.99\}$, using pseudo-observations from the baseline period which starts in 1901 (or the earliest year of the time-series, if the time-series starts later than 1901) and extends to the preceding year of the year of observations (e.g. 2024 when present-day climate is the year 2025). While the choice of using 1901 as the earliest possible start year for the time-series is somewhat arbitrary, it ensures that the time-series is sufficiently long for estimating the tails of the distribution accurately. In order to capture the extreme temperatures, the regression could be, in principle, applied to even smaller and higher quantiles (e.g. 0.001 and 0.999) if the observational time-series was long enough. However, as the shortest observed time-series in this study is 70 years, the lowest and highest quantiles will be limited to 0.01 and 0.99, respectively.

Figure 5 shows the observed 14-day running means of daily maximum temperature from 1908 to 2025 and their quantile functions for the median and selected low and high quantiles for the Sodankylä Tähtelä weather station in Finland. In general,

https://doi.org/10.5194/egusphere-2026-3721
Preprint. Discussion started: 22 July 2026

the observations exhibit a quasi-periodic seasonal cycle with the greatest inter-annual variability occurring in winter and the lowest in mid-autumn, respectively. The quantile functions capture the seasonal cycle while filtering out some of the observed short-term weather variability, such as sporadic cold spells and heatwaves. Finally, we see that the observed average daily maximum temperature between July 12th and July 25th 2025 is above the 0.99th quantile.

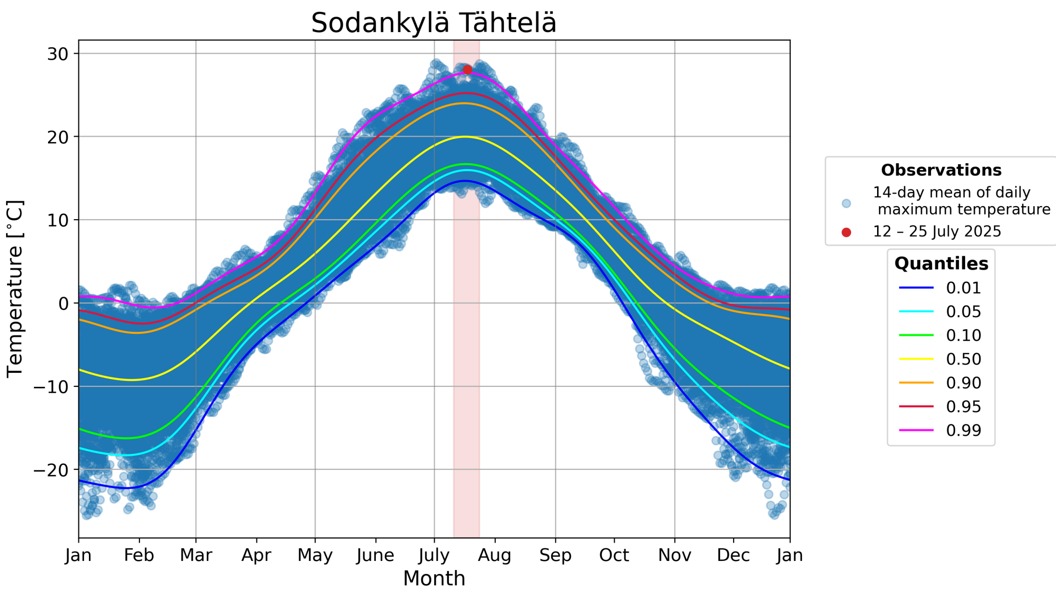

Figure 5. 14-day running mean daily maximum temperatures in Sodankylä, Finland (67.4 °N, 26.6 °E) from 1908 to 2025 (blue dots) and their quantile functions for the median (yellow) and selected low (green, cyan and blue) and high (orange, red and pink) quantiles. The observation corresponding to the heatwave of summer 2025 is highlighted with a red dot. The red shaded area highlights the time-period of the observation (12-25 July).

3.4 Continuous probability distributions

The final step in the presented attribution tool is fitting a continuous probability distribution to the 99 quantiles, corresponding to the selected time-period (the lower red box in Figure 1). The shape of the obtained quantile distribution can be skewed and long-tailed and it varies depending on the length of the period n and the time of year d. For example, in winter months the temperature distribution in Fennoscandia typically exhibits a long left tail whereas the distribution during spring and autumn months is more symmetrical. This rules out using any Gaussian-type probability distribution as it would not be able to describe the entire quantile distribution. In order to capture varying shapes of distribution accurately, we fit a 5-parametric logistic function as the cumulative distribution function (CDF) in the range of $T_{0.01} \leq T \leq T_{0.99}$. In addition, we need to describe the tail below (above) the temperature of $T_{0.01}$ ($T_{0.99}$). For these purposes, a Gumbel distribution is fitted to the left (right) tail by using temperature quantiles in the range of $T_{0.01} \leq T \leq T_{0.10}$ ($T_{0.90} \leq T \leq T_{0.99}$). While we could also fit the Generalized

https://doi.org/10.5194/egusphere-2026-3721
Preprint. Discussion started: 22 July 2026

extreme value (GEV) distribution to the tails, we use the Gumbel function as it is unrestricted and contains only two parameters instead of the three in the GEV-distribution, thus decreasing the uncertainty in fitting. The final CDF, from which a probability distribution function (PDF) can be derived, is obtained by merging the Gumbel-distributions with the logistic function. The used functions and the process of merging them are described in detail in Appendix A.

Figure 6a shows that the fitted PDF captures the shape of the frequency distribution of pseudo-observations representing 12-25th July 2025 in Sodankylä reasonably well. Figure 6b shows the PDFs, representing the pre-industrial, present-day and future climates (years 1900, 2025 and 2050 under the SSP2-4.5 scenario). The probability for the temperature being at least 28.0 °C can be visually evaluated as the area right of the vertical black line below each probability distribution function. We see that the probability for the heatwave to occur in the climate of the year 1900 is extremely small and the heatwave would also be a rare event even in the future climate of the year 2050. This highlights the fact that circulation patterns causing heatwaves of this intensity in Northern Europe are rare. Note, however, that the probability for such a heatwave occurring at any time during the summer is larger than that for a heatwave occurring during these specific days (12–25 July).

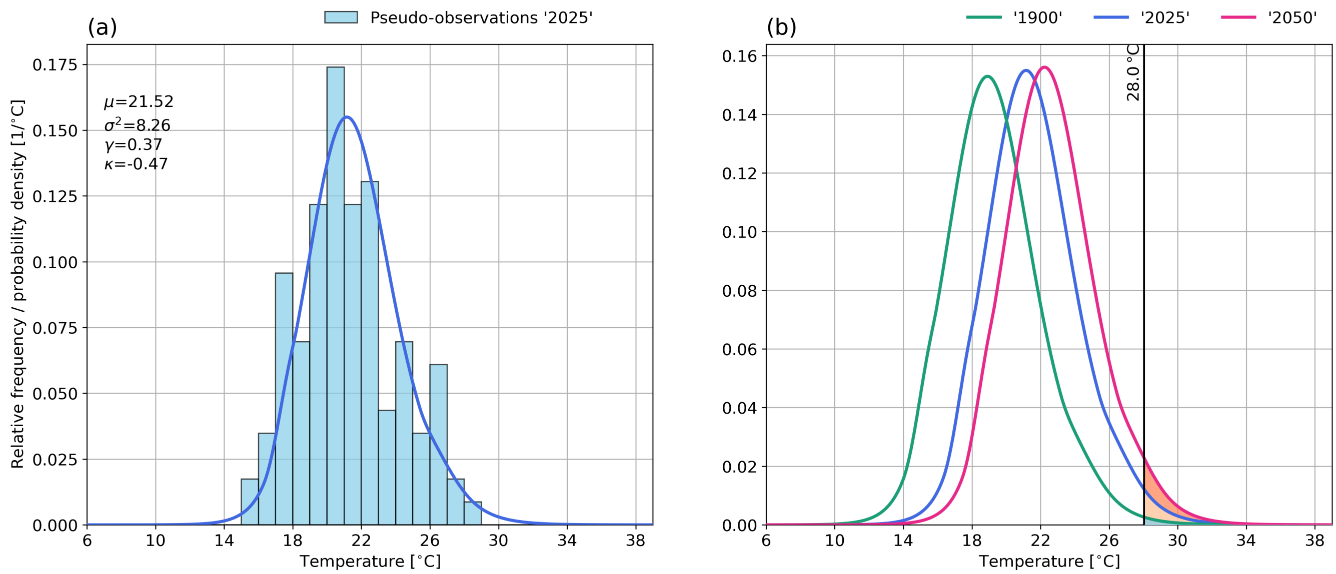

Figure 6. (a) The frequency distribution of pseudo-observations representing the 14-day average of daily maximum temperatures for the time period of 12–25 July in the climate of the year 2025 in Sodankylä, Finland. The corresponding probability distribution function is shown with a blue line. The values of the first four moments are annotated in the upper left corner of the figure. (b) Probability distribution functions for the climates of the years 1900 (green line), 2025 (blue line) and 2050 (red line) under the SSP2-4.5 scenario. The black vertical line marks the observed 14-day average of daily maximum temperatures for the time-period of 12-25 July 2025. The probability for the temperature being at least the observed 28.0 °C is shown by the shaded area right of the vertical black line below each probability distribution function.

https://doi.org/10.5194/egusphere-2026-3721
Preprint. Discussion started: 22 July 2026

3.5 Treatment of uncertainty

To account for inter-model differences, pseudo-observations are calculated separately for each model in the used CMIP6 dataset. For example, when daily maximum temperature observations are used and attribution is done with the SSP2-4.5 scenario, we get an ensemble of 29 time-series of pseudo-observations from which model-related uncertainty can be estimated (see Figure 4).

In Rantanen et al. (2024), the uncertainty associated with internal variability was assessed via a bootstrap approach, by sampling with replacement 1000 time series of pseudo-observations for each m models separately, resulting in a total of $m \cdot 1000$ realizations from which confidence intervals were calculated. However, sampling of model-specific pseudo-observations is not feasible in the current method as fitting the distribution requires performing quantile regression, which has a high computational cost. Consequently, we will first perform quantile regression to the model-specific pseudo-observations and take a random sample of 99 quantile functions with replacement. While some information is lost regarding variability and the extreme values in the tails by sampling quantile functions instead of observations, this method provides a way to account for uncertainty in internal climate variability in the range $T_{0.01} < T < T_{0.99}$. After bootstrapping model-specific quantile functions, continuous probability distributions are fitted to the daily values of quantiles. Applying this procedure 1000 times to model-specific pseudo-observations gives us a total of 29,000 realizations from which 5th and 95th percentiles are calculated.

3.6 Attribution metrics

The metrics which we use in this study for quantifying the effect of climate change on observed temperature are probability ratio (PR) and intensity change (ΔI). Probability ratio describes how much more likely the observed weather event is in the present-day climate compared to the pre-industrial climate due to climate change and is given by:

$$PR = \frac{P(T \geq T_{\text{obs}})}{P_{1900}(T \geq T_{\text{obs}})} \tag{8}$$

where $P(T \geq T_{\text{obs}})$ is the probability for the temperature being at least the observed temperature in the present-day climate and $P_{1900}(T \geq T_{\text{obs}})$ is the corresponding probability in a counterfactual climate of the year 1900, representing pre-industrial climate. Intensity change describes how much warmer the weather event is due to climate change. It is calculated by finding the percentile p of the observed temperature T_{obs} in the present-day climate and then finding the temperature corresponding to that percentile T_{1900}^{p} in the pre-industrial climate:

$$\Delta I = T_{\text{obs}} - T_{1900}^{\text{p}} \tag{9}$$

Table 1 shows the annual probabilities, return periods and temperatures for the 14-day average of daily maximum temperatures over the time-period of 12-25 July in Sodankylä, Finland. According to our best estimate, the probability for the observed heatwave to occur in Sodankylä, Finland in the present-day climate is 1.79 %, making it a 1 in 56 years event. The corresponding probability in the pre-industrial climate is 0.38 %, giving it a return period of 266 years. Thus, according to Eqs. 8 and 9,

https://doi.org/10.5194/egusphere-2026-3721
Preprint. Discussion started: 22 July 2026

climate change made the observed heatwave 4.6 (1.2–32.5) times more likely and 2.1 °C (0.3-3.3 °C) warmer. The PR and ΔI-values of individual models are shown in Figure S1. The confidence limits, shown in parentheses, were obtained by taking the 5th and 95th percentiles of 29,000 bootstrap samples. The future (2050) probability, obtained from the CMIP6-simulations forced by the SSP2-4.5 scenario, is 3.90 % corresponding to a return period of 26 years. Thus, a heatwave which would have occurred less than 4 times in a millennia in the climate of 1900, will occur approximately 4 times in a century in the climate of 2050.

Table 1. Annual probabilities, return periods and temperatures for the 14-day moving average of daily maximum temperature over the time-period of 12-25 July in Sodankylä, Finland. The values in the parentheses represent the 5th and 95th percentiles from 29,000 bootstrap samples.

Year	Probability (%)	Return period (years)	Intensity (°C)
1900	0.38 (0.03, 1.13)	264 (88, 3279)	25.9 (24.8, 27.7)
2025	1.79 (0.31, 4.97)	56 (20, 327)	28.0
2050	3.86 (0.57, 11.72)	26 (9, 177)	29.0 (28.1, 30.2)

4 Case Study: July 2025 heatwave in Fennoscandia

In this section, we apply the ATDT tool to 23 weather stations (See the used stations in Table A1) from varying locations in Fennoscandia to see how climate change affected the observed temperatures geographically during a heatwave which occurred in Northern Europe in July 2025 (Barnes et al., 2025; Copernicus Climate Change Service (C3S) and World Meteorological Organization (WMO), 2026). The attribution method is applied to the 14-day averages of daily maximum and minimum temperatures over the time-periods of 12-25 July and 19 July - 1 August, as these periods corresponded to the annual maximums of 14-day average maximum and minimum temperatures, averaged over the contiguous region of mainland Norway, Sweden and Finland, and they are the same periods used in the World Weather Attribution analysis by Barnes et al. (2025). For the sake of brevity, the local station-specific 14-day averages of daily maximum and minimum temperatures will be referred to hereafter as Tx14 and Tn14, respectively.

Figure 7 shows the Tx14 and Tn14 observations (panels a-b) together with their corresponding deviations from their 30-year (1991-2020) baseline climatologies (panels c-f). Tx14 observations were highest at the respective station's history for the time-period of 12-25 July at all stations in Central and Northern Sweden and at all Norwegian weather stations South of 70 °N. In contrast, a record Tn14 observation was set at only five weather stations. Note that these values represent records for the respective time periods, not all-time Tx14 or Tn14 records at the stations. Figures 7c-d show that the magnitudes of temperature anomalies reached up to 11.0 °C for Tx14 and 4.6 °C for Tn14. Thus, the temperature anomalies were greater for Tx14 than for Tn14 at all weather stations. The normalized anomalies (in standard deviations) were also greater for Tx14 than Tn14 at all

https://doi.org/10.5194/egusphere-2026-3721
Preprint. Discussion started: 22 July 2026

stations except at Lund, Southernmost Sweden (Figures 7e-f). The most extreme temperatures were observed at the Norwegian stations of Værnes, Tafjord and Flesland and at Kvikkjokk, Sweden where the local temperature anomalies were 4.5 or 3.6 standard deviations above their climatological mean values.

Figures 8a-b show the calculated intensity changes for Tx14 and Tn14 (For uncertainty estimates of ΔI, see Figure S2). We see that climate change made the observed temperatures 1.4 to 2.4 °C warmer compared to the climate of 1900. Tx14 temperatures were warmed more than the Tn14 temperatures at all stations except at the Norwegian stations of Tafjord and Vardø and Swedish station Kvikkjokk-Årrenjarka. This is because the local 14-day average maximum temperatures for the time-period 12–25 July are projected to warm more than the local 14-day average minimum temperatures for the time-period 19 July–1 August in most areas of Fennoscandia according to the ensemble of CMIP6 models we have used (Figure A2). We also see from Figure 8a that the intensity change of Tx14 increases eastward and northward of Western Norway. The spatial distribution of ΔI is qualitatively similar for Tn14.

The probability of temperatures reaching at least the observed Tx14 and Tn14 values in the climate of the year 1900 is shown in Figures 8c-d. The estimated probability for the observed Tx14 is between 0.01 and 0.10 % at seven weather stations, corresponding to 1-in-1000 year to 1-in-10,000 year events, highlighting how extremely rare the observed heatwave would have been in a pre-industrial climate. The estimated probability is between 0.11 and 1.0 % at 11 other stations and between 1.1 and 9.7 % at five stations. In terms of Tn14, the estimated probability for the observed temperatures is below 0.10 % at only 2 stations, between 0.1 % and 1.0 % at 16 stations and between 1.1 and 11.4 % at 5 stations, respectively. The median probability of occurrence over all stations is slightly smaller for Tx14 (0.2 %) than it is for Tn14 (0.4 %).

Figures 8e-f show the calculated PRs for Tx14 and Tn14 (For uncertainty estimates of PR, see Figure S3). Climate change has increased the probability of the local Tx14 (Tn14) event by a factor ranging from 3.0 to 14.6 (6.1 to 22.9) compared to the climate of 1900. The PRs of both Tx14 and Tn14 tend to increase southward from northern Norway, with the highest PRs obtained for coastal stations, such as, Færder Fyr, Norway; Göteborg, Sweden and Helsinki, Finland. In addition, the PRs of Tn14 exceed those of Tx14 at all stations, except at Sauda, Southwestern Norway. The reason why coastal stations and Tn14 obsrvations have higher PRs is their smaller inter-annual variability compared to the continental and Tx14 observations, leading to a narrower probability distribution and thus higher probability in the present-day climate. For example, the average standard deviation of Tx14 pseudo-observations in the year 2025 is 2.4 °C, while that of Tn14 observations is 1.5 °C. Other factors affecting probabilities in the year 1900 and PRs include the regression coefficients $\langle B_{14} \rangle$ and $\langle D_{14} \rangle$, the shape of the distribution near the upper tail and the extremity of the observed temperature.

The calculated ΔIs and PRs are in qualitative agreement with the observed temperature trends in Fennoscandia. For example, extremely warm months (defined as three standard deviations above the average of the time-series) in Sweden have been most frequent in the last 30 years of the period 1860-2021 (Joelsson et al., 2023). Other studies also highlight that extreme summer

https://doi.org/10.5194/egusphere-2026-3721
Preprint. Discussion started: 22 July 2026

temperatures have become warmer elsewhere in Fennoscandia (Kivinen et al., 2017; Sulikowska and Wypych, 2021; Rantanen et al., 2025).

Finally, in order to get an estimate for the Tx14 and Tn14 event in intensities and frequencies in a future climate, represented by the year 2050, we calculated how many degrees warmer the local Tx14 and Tn14 would be compared to the observations made in 2025 (Figures 9a-b) and how much more likely the observed temperatures would be in 2050 compared to 2025 (Figures 9c-d). The intensity changes between the climates of 2050 and 2025 exhibit similar patterns as the intensity changes between the climates of 2025 and 1900, shown in Figures 8c-d; the Tx14 temperatures are warmed more than the Tn14 temperatures with the smallest warming projected to occur in Western Norway. Thus, a heatwave of similar magnitude is projected to be 0.7–0.8 °C warmer in Western Norway and approximately 1 °C warmer in most other areas of Fennoscandia compared to the climate of 2025. It is also worth noting that the 14-day average minimum temperature is projected to be 20.1 ° in Helsinki, Finland in 2050, exceeding the threshold for a tropical nighttime temperature (nighttime minimum temperature > 20 °C) (See Figures 7b and 9b). The local probability of the observed Tx14 and Tn14 temperature is projected to increase by a factor of 1.6 to 4.4 and 1.4 to 5.2 compared to the climate of 2025 with the probability of Tn14 temperature increasing more. The median probability ratios over all 23 stations are 2.1 for Tx14 and 2.6 for Tn14.

4.1 Inter-method comparison of attribution results

Shortly after the heatwave had occurred, World Weather Attribution (WWA) published a scientific report on the impact of climate change on it (Barnes et al., 2025). The attribution of the event was done according to the methodology proposed by Philip et al. (2020). The effect of climate change was quantified by a fitting non-stationary GEV-function to the warmest 14-day average maximum and minimum temperatures events over Fennoscandia separately for observations and two model datasets (CMIP6 & Euro-CORDEX (Jacob et al., 2014)), by using a 4-year moving average of the global mean surface temperature as a co-variate. Following this, probability ratio and intensity change were calculated separately for each dataset and the final synthesized results were obtained by taking an average over the individual dataset-specific values. The report concluded that climate change made the annual maximums of 14-day maximum and minimum temperature events over the contiguous region of Fennoscandia 2.0 and 1.9 °C warmer and 7.4 and 33 times more likely compared to a 1.3 °C cooler counterfactual climate. However, the inter-dataset differences in the estimated probability ratio were extremely wide ranging from 5.3, when the Euro-CORDEX dataset was used, to infinite when observations were used, highlighting the large uncertainty in estimating PR. The corresponding inter-dataset difference for ΔI was 0.8 °C (Barnes et al., 2025).

As the WWA-report estimated the average ΔI and PR over the entire contiguous region of Fennoscandia while we estimated the same metrics for individual weather stations, we cannot compare our results to theirs directly. However, we see that the local values of ΔI for both Tx14 and Tn14 in this study are within the confidence intervals of the regional aggregate ΔIs of the WWA-study, and are approximately of similar magnitude. In terms of PR, our results agree qualitatively with those in Barnes et al. (2025) in the sense that PR is greater for the 14-day average minimum than the 14-day average maximum

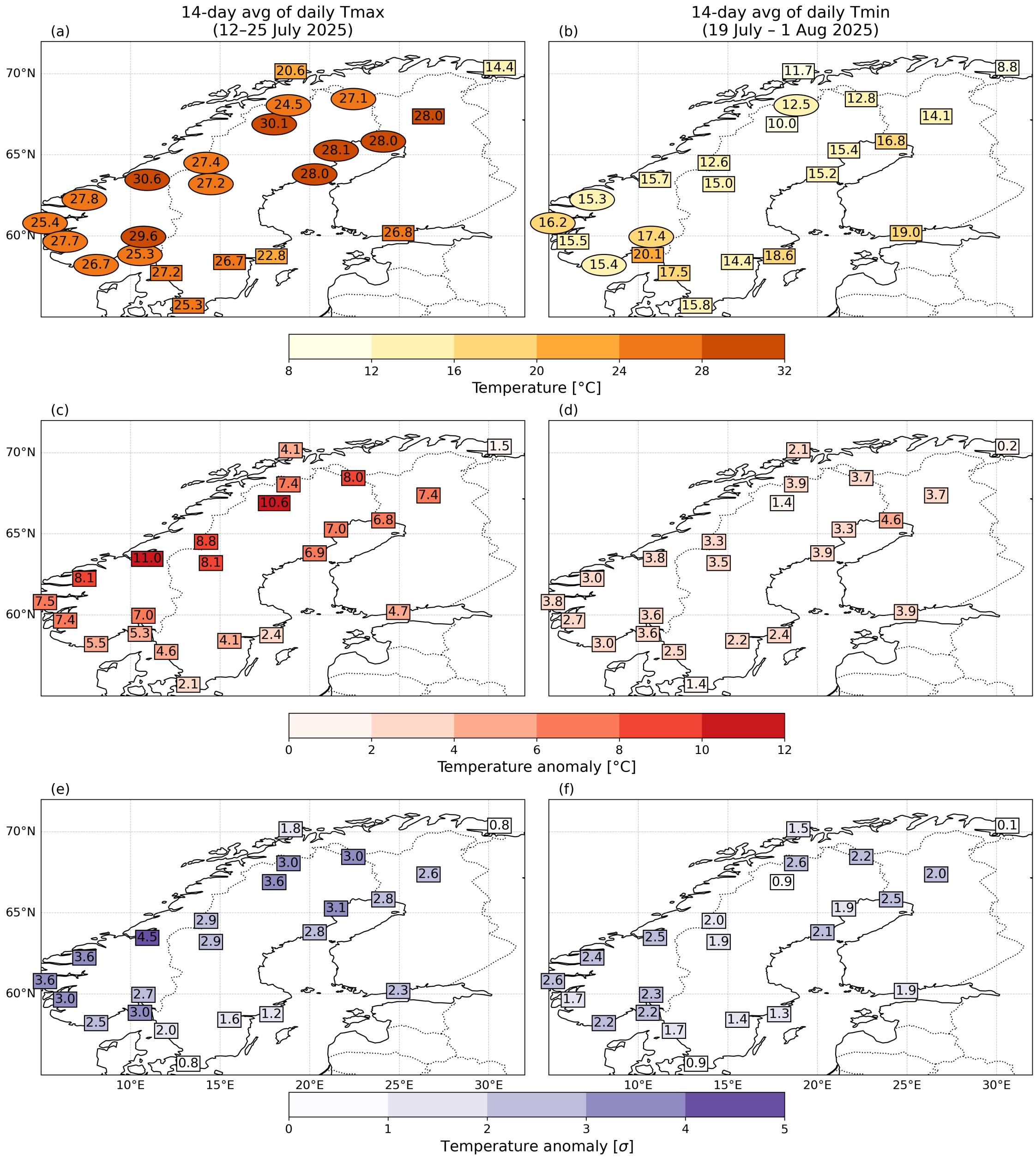

Figure 7. 14-day moving averages of *in-situ* (a) daily maximum temperature observations for the time-period of 12–25 July, 2025 (b) daily minimum temperature observations for the time-period of 19 July–1 August, 2025. Stations where record temperatures were set are elliptical. The corresponding deviations from the baseline climatology of 1991-2020 in °C (c)-(d) and in standard deviations (e)-(f).

https://doi.org/10.5194/egusphere-2026-3721
Preprint. Discussion started: 22 July 2026

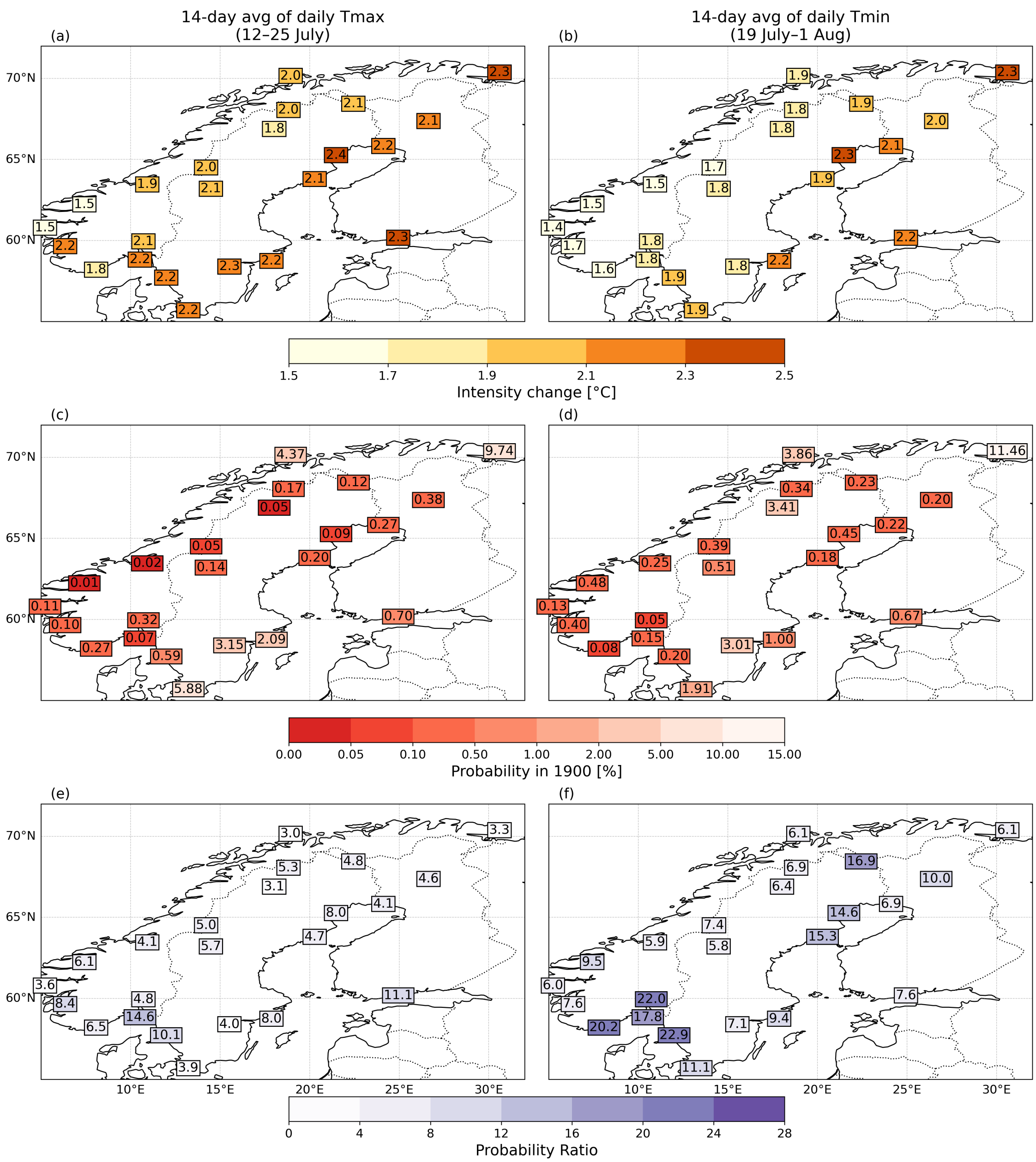

Figure 8. The station-specific values of intensity change (a)-(b), probability in the year 1900 (c)-(d) and probability ratio (e)-(f). The left column corresponds to the 14-day moving average of daily maximum temperature observations for the time-period of 12–25 July, 2025 and the right column to the 14-day moving average of daily minimum temperature observations for the time-period of 19 July–1 August, 2025.

https://doi.org/10.5194/egusphere-2026-3721
Preprint. Discussion started: 22 July 2026

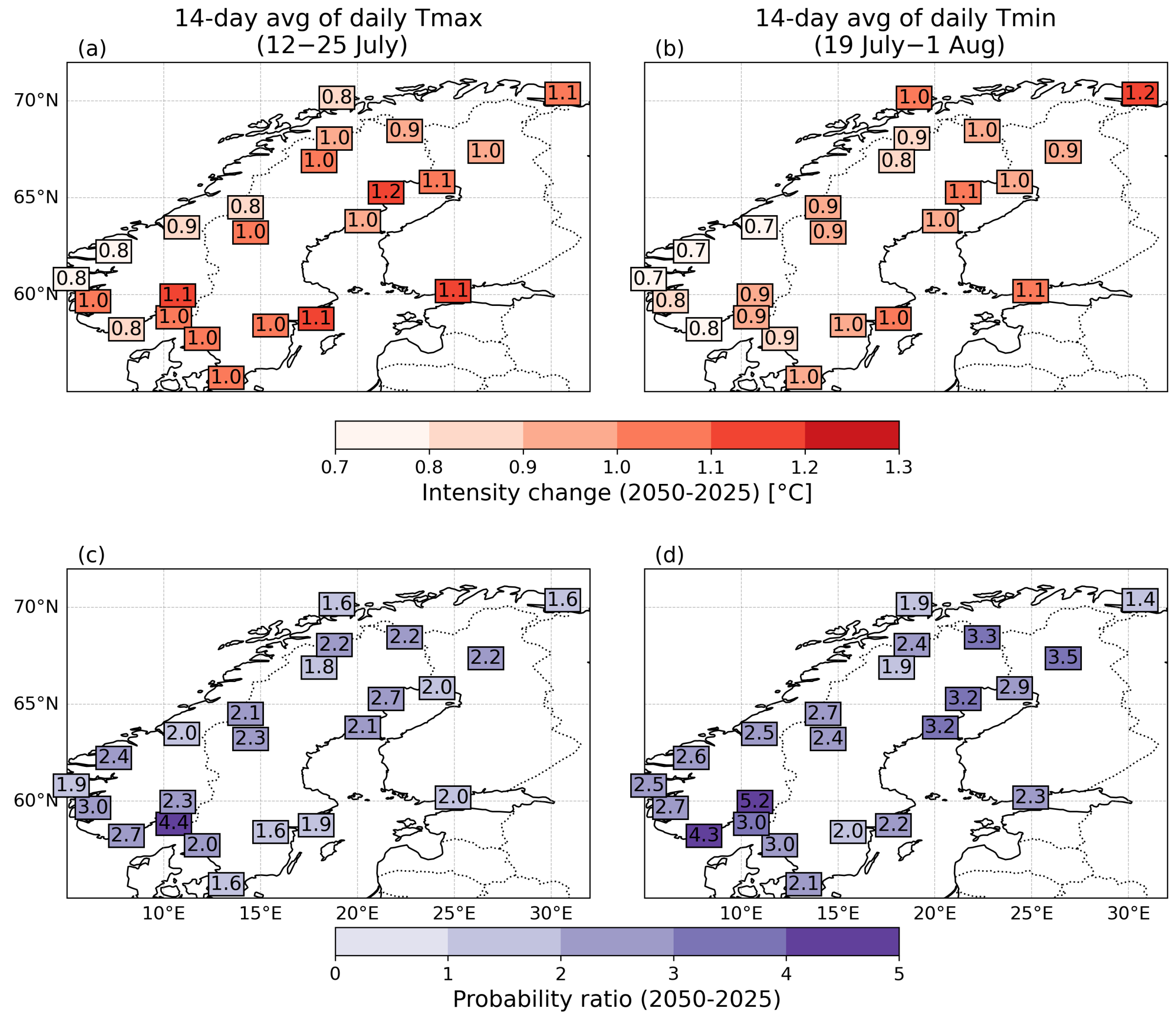

Figure 9. The station-specific values of intensity change (a-b) and probability ratio (c-d) between the years 2050 and 2025.

https://doi.org/10.5194/egusphere-2026-3721
Preprint. Discussion started: 22 July 2026

temperature. One reason why the PRs in the WWA-report are higher is that they were calculated as an aggregate over the entire Fennoscandian region, which increases the signal-to-noise ratio and thus probability ratio (Fischer et al., 2018; Uhe et al., 2016). We should also note that estimating the probability of an extremely rare weather event, such as the Fennoscandian heatwave of 2025, is highly sensitive to the method by which a distribution is fitted to the dataset, increasing uncertainty in probability ratio.

5 Discussion

Climate change attribution methods are typically applied to extremely anomalous weather events, such as the Fennoscandian Heatwave of July 2025. For this event, our new attribution tool estimates that anthropogenic climate warming since 1900 increased the intensity of the heatwave by approximately 1.4–2.4 °C relative to a counterfactual 1900 climate. Interestingly, the magnitude of the intensity change is generally smallest in the regions where the heatwave itself was most intense, particularly western and central Norway (Figs. 7–8). This spatial pattern is primarily explained by the relatively weaker warming projected by CMIP6 models over the Norwegian Sea and adjacent coastal regions compared to eastern Fennoscandia (See Figure A2). Nevertheless, the fact that the smallest intensity changes occur where the heatwave was most intense may be initially counterintuitive. However, it highlights that the local intensity of a heatwave does not directly reflect the magnitude of the anthropogenic climate change contribution, and should not be interpreted as such.

Our results should be viewed in the context of observational and methodological uncertainties. Consequently, the first source of uncertainty of this attribution method, and those of many others, is obtaining a sufficiently long time-series of observations for the purpose of reliably estimating the probability distribution near the tails of the distribution. If the time-series is too short, it may not contain sufficiently many extreme temperature events, leading to erroneous estimation of the shape of the distribution, affecting the calculated PR. According to van Oldenborgh et al. (2021), observational time-series should be at least 50 years and ideally more than 100 years long. We have used 23 observational time-series which are at least 70 years long, with three of them being longer than 100 years (See Table A1).

A second source of uncertainty, specific to this attribution method, arises from fitting a continuous probability distribution to quantiles in the range 0.01...0.99, increasing the uncertainty of estimating the probability of those events which fall outside this range (See sections 3.3–3.4 and Appendix A). One potential option of better capturing the most extreme events would be to estimate the regression coefficients and fit the probability distribution separately for specific subsets of extremes, such as annual maxima and minima, or for event-based definitions of extremes (e.g. the warmest 3/5/7/14-day periods of the summer), rather than using a fixed 14-day window anchored to observed calendar dates. This type of approach was used in the WWA analysis (Barnes et al., 2025), as it allows the most extreme heatwave to occur at any time within the season. However, the current fixed-window approach also has advantages, particularly in transitional seasons (spring and autumn), when restricting the analysis to a predefined temporal window is essential as it reduces contamination from events occurring in clearly different

https://doi.org/10.5194/egusphere-2026-3721
Preprint. Discussion started: 22 July 2026

parts of the seasonal cycle.

A third source of uncertainty in the described method comes from the model errors and limited resolution of the CMIP6-models from which the regression coefficients are estimated. These regression coefficients could be, in principle, calculated also from observations. Hence, one potential direction for future development would be to move beyond regression coefficients that are purely derived from CMIP6-simulations, and explore weighted approaches that combine the model-based climate change estimates with information from local observed temperature trends (Räisänen et al., 2025). Such an approach could reduce the influence of potential CMIP6 biases in regional warming patterns, and provide more realistic estimates of local climate responses to global warming. In addition, the regression equations (Eqs. 2 and 3) imply that the local changes in mean and variance in response to global warming, stay constant over time. However, this may not be true if the realized changes in the climate are large or if the balance of different forcing factors, such as, global greenhouse gas and regional aerosol forcings, changes over time (Wells et al., 2023).

A final source of uncertainty in the proposed method is the underlying assumption that climate change will not alter the shape of the probability distribution, except for mean and variance. According to the supplementary analysis in Rantanen et al. (2024), skewness and kurtosis of monthly mean temperatures in CMIP6 simulations change significantly between the time-periods of 1901-1950 and 2051-2100 only in specific regions such as the Arctic Ocean. However, currently we do not know if this holds true in sub-monthly time-scales. For example, during spring, reductions in seasonal snow cover and sea ice may alter the shape of the temperature distribution. Such effects are not explicitly represented in the present method.

In order to evaluate and reduce uncertainty in the obtained attribution results, we plan to conduct a probabilistic verification study of the method's performance in predicting the locally observed climate in the future. The verification scores calculated in Räisänen and Ruokolainen (2008a) and Räisänen et al. (2025) showed that, on monthly time-scales, the attribution method is able to predict the locally observed climate better than past observations alone. The results of Räisänen et al. (2025) also suggest that, at least for monthly mean temperatures, the performance of the method can be further improved by replacing the model-based regression coefficients by an approximately equally weighted average of the model- and observation based coefficients.

6 Conclusions

In this paper, we have described the ATDT attribution tool which enables meteorologists and scientists to estimate the effect of climate change on local daily mean, maximum and minimum temperature observations or their 2 to 31-day moving averages in near-real-time. The proposed method uses CMIP6-model simulations and daily mean, maximum and minimum temperature observations and is an extension to the previously published versions of this tool (Räisänen and Ruokolainen, 2008a, b; Rantanen et al., 2024) which were used to attribute monthly, seasonal and annual mean temperatures to climate change. The tool

https://doi.org/10.5194/egusphere-2026-3721
Preprint. Discussion started: 22 July 2026

described in this paper is planned to be used in an operational attribution service at the Finnish Meteorological Institute.

We demonstrated the tool with the 14-day averages of daily maximum and minimum temperature observations from 23 weather stations in Fennoscandia for the time-periods of 12–25 July, 2025 and 19 July–1 August, 2025 when an exceptionally intense heatwave affected Northern Europe. We find that the station-specific average maximum temperatures were made 1.5 to 2.4 °C and the minimum temperatures 1.4 to 2.3 °C warmer compared to the near-preindustrial climate of the year 1900. Furthermore, these temperatures were made 3.0–14.6 times (maximum temperature) and 6.1–22.9 times (minimum temperature) more likely by climate change since the year 1900.

Code and data availability. The code and data needed to produce the results are available in Zenodo: https://doi.org/10.5281/zenodo.20742664 Toropainen et al. (2026). Station observations from Finland, Sweden and Norway are available through each country's national weather service open data portals (Finland: https://en.ilmatieteenlaitos.fi/open-data, Sweden: https://www.smhi.se/data/hitta-data-for-en-plats/ladda-ner-vaderobservationer/, Norway: https://seklima.met.no/). CMIP6 data are available from Earth System Grid Federation (ESGF) archive at: https://metagrid.esgf-west.org/search/cmip6/.

Author contributions. AT was the main developer of the software, produced the results, prepared the figures and was the lead writer of the manuscript. MR contributed in developing the software, writing, reviewing and editing the manuscript and supervision. JR conceptualized the methodology and contributed in reviewing and editing the manuscript and supervision. All authors have read, commented and approved the final manuscript.

Competing interests. The authors declare that they have no conflict of interest.

Acknowledgements. This research has been supported by the CLAIMS consortium, funded by Academy of Finland (Decision numbers 362263 and 362264). We thank the CSC—Finnish IT Center for access to computer clusters and data storage. We thank the individual climate modeling groups for making their model outputs available, the Earth System Grid Federation (ESGF) for archiving the data and all funding agencies who support CMIP6 and ESGF. We also thank Amalie Skålevåg for helping us access observations from Norwegian Meteorological Institute.

Appendix A: Details of curve fitting

The 5-parameter logistic function CDF which we fit to the quantiles corresponding to the selected weather station and time-period (e.g. Helsinki, Finland on Jan 1st) has the form:

https://doi.org/10.5194/egusphere-2026-3721
Preprint. Discussion started: 22 July 2026

$$F_{\mathrm{L}}(T) = A + \frac{D-A}{\Big(1+\exp\big(B(C-T)\big)\Big)^{\mathrm{S}}}, \qquad T_{0.01} \leq T \leq T_{0.99} \tag{A1}$$

where A, B, C, D and S are parameters that govern the shape of the function and T is temperature. Although the 5-parameter logistic function has been typically used in medical studies to model, for example, baroreflex curves (Ricketts and Head, 1999) and dose-response (Gottschalk and Dunn, 2005; Liao and Liu, 2009), the 5-parametric logistic function can also be fitted to a set of temperature quantiles under some constraints for the parameters. The parameters A and D are the horizontal asymptotes when the response variable (T in this case) approaches $-\infty$ and ∞, respectively. In this study, however, the parameters A and D are constrained so that they correspond to the horizontal asymptotes of T approaching $T_{0.01}$ and $T_{0.99}$, respectively. Consequently, $D > A$ in all cases. Parameter B governs the rate at which the curve transitions between the horizontal asymptotes A and D. In the case that $D > A$, parameter B must be positive as the fitted CDF must have a positive slope. Parameter C is the location parameter. When the curve is symmetric (S = 1), C corresponds to the temperature at which the curve has an inflection point. Finally, parameter S governs the symmetry of the curve. The optimal parameters are estimated by using the curve_fit function available in Python's Scipy-library. The PDF is obtained by taking the derivative of Eq. (A1) with respect to T:

$$f_{\mathrm{L}}(T) = (D-A)\,SB\,\frac{\exp\big(B(C-T)\big)}{\Big(1+\exp\big(B(C-T)\big)\Big)^{S+1}}, \qquad T_{0.01} \leq T \leq T_{0.99} \tag{A2}$$

After optimizing the parameters of the logistic function and obtaining a CDF for the range $T_{0.01} < T < T_{0.99}$, we fit CDFs of the Gumbel distribution to the left and right tails by using the ten highest and lowest quantiles. The CDFs of Gumbel-distribution for the right and left tails are given by:

$$F_{\max}(T) = \exp\left(-\exp\left(-\frac{T-\mu_{\max}}{\beta_{\max}}\right)\right), \qquad T_{0.90} \leq T \leq T_{0.99} \tag{A3}$$

$$F_{\min}(T) = 1-\exp\left(-\exp\left(\frac{T-\mu_{\min}}{\beta_{\min}}\right)\right), \qquad T_{0.01} \leq T \leq T_{0.10} \tag{A4}$$

where μ and β are the location and scale parameters, respectively. The corresponding PDFs are given by:

$$f_{\max}(T) = \frac{1}{\beta_{\max}}\exp\left(-\frac{T-\mu_{\max}}{\beta_{\max}}\right)\exp\left(-\exp\left(-\frac{T-\mu_{\max}}{\beta_{\max}}\right)\right), \qquad T_{0.90} \leq T \leq T_{0.99} \tag{A5}$$

$$f_{\min}(T) = \frac{1}{\beta_{\min}}\exp\left(\frac{T-\mu_{\min}}{\beta_{\min}}\right)\exp\left(\exp\left(\frac{T-\mu_{\min}}{\beta_{\min}}\right)\right), \qquad T_{0.01} \leq T \leq T_{0.10} \tag{A6}$$

The parameters $\mu_{\min}$, $\mu_{\max}$, $\beta_{\max}$ and $\mu_{\max}$ in the Gumbel distributions are derived by imposing two constraints. First, in the case of the left (right) tail, the logistic function CDF at the 0.05th (0.95th) quantile must be equal to the Gumbel-distribution CDF at the 0.05th (0.95th) quantile. Second, in the case of the left (right) tail, the derivative of the logistic function CDF at the

https://doi.org/10.5194/egusphere-2026-3721
Preprint. Discussion started: 22 July 2026

0.05th (0.95th) quantile must be equal to the derivative of the 0.05th (0.95th) quantile of the Gumbel-distribution CDF. These constraints can be expressed as two pairs of equations:

$$\begin{cases} F_{\min}(T_{0.05}) = 1 - \exp\left(-\exp\left(\dfrac{T_{0.05}-\mu_{\min}}{\beta_{\min}}\right)\right) = F_{\mathrm{L}}(T_{0.05}) \\ f_{\min}(T_{0.05}) = \dfrac{1}{\beta_{\min}}\exp\left(\dfrac{T_{0.05}-\mu_{\min}}{\beta_{\min}}\right)\exp\left(-\exp\left(\dfrac{T_{0.05}-\mu_{\min}}{\beta_{\min}}\right)\right) = f_{\mathrm{L}}(T_{0.05}) \end{cases} \tag{A7a}$$

$$\begin{cases} F_{\max}(T_{0.95}) = \exp\left(-\exp\left(-\dfrac{T_{0.95}-\mu_{\max}}{\beta_{\max}}\right)\right) = F_{\mathrm{L}}(T_{0.95}) \\ f_{\min}(T_{0.95}) = \dfrac{1}{\beta_{\max}}\exp\left(-\dfrac{T_{0.95}-\mu_{\max}}{\beta_{\max}}\right)\exp\left(-\exp\left(-\dfrac{T_{0.95}-\mu_{\max}}{\beta_{\max}}\right)\right) = f_{\mathrm{L}}(T_{0.95}) \end{cases} \tag{A7b}$$

Now, by solving Equations A7a and A7b, we get the following expressions for the parameters μ and β for the left and right tails:

$$\begin{cases} \mu_{\min} & = T_{0.05} - \frac{\left(1-F_{\mathrm{L}}(T_{0.05})\right)}{f(T_{0.05})}\ln\left(\frac{1}{1-F_{\mathrm{L}}(T_{0.05})}\right)\cdot\ln\left(\ln\left(\frac{1}{1-F_{\mathrm{L}}(T_{0.05})}\right)\right) \\ \beta_{\min} & = \frac{\left(1-F_{\mathrm{L}}(T_{0.05})\right)}{f(T_{0.05})}\ln\left(\frac{1}{1-F_{\mathrm{L}}(T_{0.05})}\right) \end{cases} \tag{A8a}$$

$$\begin{cases} \mu_{\max} & = T_{0.95} + \frac{F_{\mathrm{L}}(T_{0.95})}{f(T_{0.95})}\ln\left(\frac{1}{F_{\mathrm{L}}(T_{0.95})}\right)\cdot\ln\left(\ln\left(\frac{1}{F_{\mathrm{L}}(T_{0.95})}\right)\right) \\ \beta_{\max} & = \frac{F_{\mathrm{L}}(T_{0.95})}{f(T_{0.95})}\ln\left(\frac{1}{F_{\mathrm{L}}(T_{0.95})}\right) \end{cases} \tag{A8b}$$

After the parameters are obtained for both Gumbel distributions, they are merged with the logistic function CDF $F_{\mathrm{L}}(T)$ by using the Smoothstep function:

$$S(x) = 3x^2 - 2x^3, \quad 0 \le x \le 1 \tag{A9}$$

where x is defined as follows:

$$x = \begin{cases} \frac{T-T_{0.01}}{T_{0.10}-T_{0.01}}, & T_{0.01} \le T \le T_{0.10} \\ \frac{T-T_{0.90}}{T_{0.99}-T_{0.90}}, & T_{0.90} \le T \le T_{0.99} \end{cases} \tag{A10}$$

After merging, we obtain the final forms for CDF $F(T)$ and PDF $f(T)$:

$$F(T) = \begin{cases} F_{\min}(T), & \text{if } T \le T_{0.01} \\ (1-S(x))\cdot F_{\min}(T) + S(x)\cdot F_{\mathrm{L}}(T), & \text{if } T_{0.01} \le T \le T_{0.10} \\ F_{\mathrm{L}}(T), & \text{if } T_{0.10} \le T \le T_{0.90} \\ (1-S(x))\cdot F_{\mathrm{L}}(T) + S(x)\cdot F_{\max}(T), & \text{if } T_{0.90} \le T \le T_{0.99} \\ F_{\max}(T), & \text{if } T \ge T_{0.99} \end{cases} \tag{A11}$$

$$f(T) = \begin{cases} f_{\min}(T), & \text{if } T \leq T_{0.01} \\ (1-S(x)) \cdot f_{\min}(T) + S(x) \cdot f_{\mathrm{L}}(T), & \text{if } T_{0.01} \leq T \leq T_{0.10} \\ f_{\mathrm{L}}(T), & \text{if } T_{0.10} \leq T \leq T_{0.90} \\ (1-S(x)) \cdot f_{\mathrm{L}}(T) + S(x) \cdot f_{\max}(T), & \text{if } T_{0.90} \leq T \leq T_{0.99} \\ f_{\max}(T), & \text{if } T \geq T_{0.99} \end{cases} \tag{A12}$$

Figure A1a shows 99 quantiles and the fitted CDF corresponding to daily mean temperature observations from Helsinki Kaisaniemi, Finland on Jan 1st. This location and day-of-year were selected as the corresponding quantile distribution is asymmetric and has a long left tail. Despite of the asymmetry, the CDF seems to fit the quantile distribution reasonably well, with some small under-fitting occurring in the long left tail. In addition, merging of $F_{\mathrm{L}}(T)$ to $F_{\min}(T)$ and $F_{\max}(T)$ is smooth enough so that a smooth PDF is obtained, as is evident in Figure A1b.

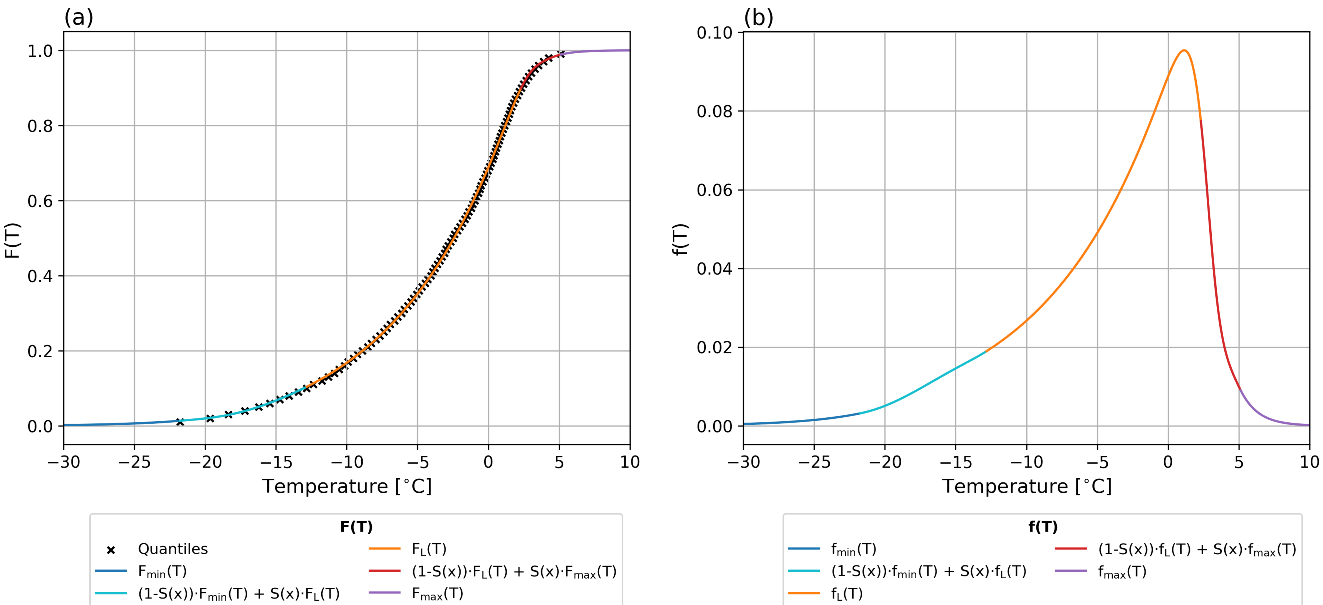

Figure A1. 99 quantiles and 5 parts of the CDF (a) and PDF (b) according to Eqs. A11– A12. The quantiles have been obtained by performing QR to daily mean temperature observations from Helsinki Kaisaniemi, Finland and selecting the quantiles that correspond to Jan 1st.

https://doi.org/10.5194/egusphere-2026-3721
Preprint. Discussion started: 22 July 2026

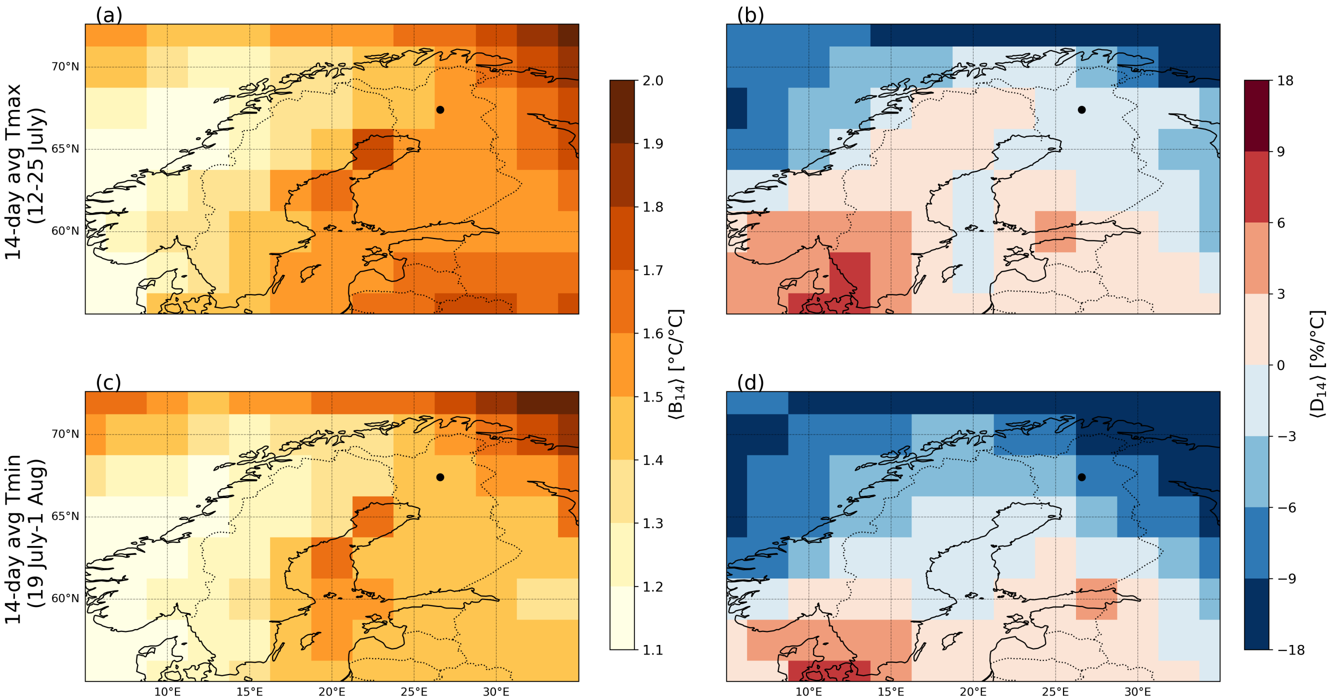

Figure A2. Multi-model mean regression coefficients $\langle B_{14} \rangle$ (panels a) and c)) and $\langle D_{14} \rangle$ (panels b) and d)) for the 14-day average maximum and minimum temperatures over the time-periods of 12–25 July and 19 July–1 August.

https://doi.org/10.5194/egusphere-2026-3721
Preprint. Discussion started: 22 July 2026

Table A1. Weather stations from Nordic countries that were used in estimating the effect of climate change on the heatwave which occurred in July, 2025. FMI stands for the Finnish Meteorological Institute and SMHI for the Swedish Meteorological and Hydrological Institute and METNO for Norwegian Meteorological Institute, respectively. Station ID refers to the ID-number of the station, designated by the data provider. Nine observational time-series provided by SMHI were formed by concatenating the time-series of an older non-active weather station to that of a newer active nearby station. The corresponding station IDs are separated by the & sign in the Station ID column while the Station name column shows the name of the newest active station.

Data provider	Station ID(s)	Station name	Latitude (°N)	Longitude (°E)	Time-series length (years)
FMI	100971	Helsinki, Kaisaniemi	60.18	24.95	125
FMI	101932	Sodankylä, Tähtelä	67.38	26.63	118
SMHI	87450	Landsort	58.740	17.866	85
SMHI	53430	Lund	55.693	13.225	81
SMHI	161790	Piteå	65.263	21.474	85
SMHI	188800 & 188790	Abisko Aut	68.354	18.816	70
SMHI	144300 & 144310	Gäddede A	64.504	14.221	85
SMHI	72630 & 71420	Göteborg A	57.716	11.992	76
SMHI	163950 & 163960	Haparanda A	65.837	24.113	85
SMHI	192830 & 192840	Karesuando A	68.442	22.444	83
SMHI	167980 & 167990	Kvikkjokk-Årrenjårkå A	66.887	18.02	86
SMHI	85250 & 85240	Linköping-Malmslätt	58.398	15.523	85
SMHI	140500 & 140480	Umeå Airport	63.793	20.28	85
SMHI	134100 & 134110	Östersund-Frösön Airport	63.198	14.487	85
METNO	SN27500	Færder, Fyr	59.027	10.524	89
METNO	SN50500	Flesland	60.2892	5.2265	70
METNO	SN39040	Kjevik	58.2	8.0767	80
METNO	SN18700	Oslo, Blindern	59.973	10.710	89
METNO	SN46610	Sauda	59.6479	6.3499	92
METNO	SN60500	Tafjord	62.231	7.422	70
METNO	SN90450	Tromsø	69.654	19.937	101
METNO	SN69100	Værnes	63.496	10.931	80
METNO	SN98550	Vardø radio	70.371	31.096	93

https://doi.org/10.5194/egusphere-2026-3721
Preprint. Discussion started: 22 July 2026

References

Athanase, M., Sánchez-Benítez, A., Monfort, E., Jung, T., and Goessling, H. F.: How climate change intensified storm Boris' extreme rainfall, revealed by near-real-time storylines, Commun. Earth Environ., 5, 676, 2024.

Barbosa, S. M.: Quantile trends in Baltic sea level, Geophysical Research Letters, 35, https://doi.org/https://doi.org/10.1029/2008GL035182, 2008.

Barbosa, S. M., Scotto, M. G., and Alonso, A. M.: Summarising changes in air temperature over Central Europe by quantile regression and clustering, Natural Hazards and Earth System Sciences, 11, 3227–3233, https://doi.org/10.5194/nhess-11-3227-2011, 2011.

Barnes, C., Clarke, B., Rantanen, M., Skålevåg, A., Ødemark, K., Kjellström, E., Vahlberg, M., Singh, R., Otto, F., Zachariah, M., and et al.: Intense two-week heatwave in Fennoscandia hotter and more likely due to climate change, https://doi.org/10.25560/122924, 2025.

Calvo-Sancho, C., Díaz-Fernández, J., González-Alemán, J. J., Halifa-Marín, A., Miglietta, M. M., Azorin-Molina, C., Prein, A. F., Montoro-Mendoza, A., Bolgiani, P., Morata, A., and Martín, M. L.: Human-induced climate change amplification on storm dynamics in Valencia's 2024 catastrophic flash flood, Nat. Commun., 17, 1492, 2026.

Copernicus Climate Change Service (C3S), E. and World Meteorological Organization (WMO): European State of the Climate 2025, https://doi.org/10.24381/zy93-sb27, 2026.

Donat, M. G., Alexander, L. V., Yang, H., Durre, I., Vose, R., Dunn, R. J. H., Willett, K. M., Aguilar, E., Brunet, M., Caesar, J., Hewitson, B., Jack, C., Klein Tank, A. M. G., Kruger, A. C., Marengo, J., Peterson, T. C., Renom, M., Oria Rojas, C., Rusticucci, M., Salinger, J., Elrayah, A. S., Sekele, S. S., Srivastava, A. K., Trewin, B., Villarroel, C., Vincent, L. A., Zhai, P., Zhang, X., and Kitching, S.: Updated analyses of temperature and precipitation extreme indices since the beginning of the twentieth century: The HadEX2 dataset, Journal of Geophysical Research: Atmospheres, 118, 2098–2118, https://doi.org/https://doi.org/10.1002/jgrd.50150, 2013.

Duan, Q., McGrory, C. A., Brown, G., Mengersen, K., and Wang, Y.-G.: Spatio-temporal quantile regression analysis revealing more nuanced patterns of climate change: A study of long-term daily temperature in Australia, PLOS ONE, 17, 1–16, https://doi.org/10.1371/journal.pone.0271457, 2022.

Eyring, V., Bony, S., Meehl, G. A., Senior, C. A., Stevens, B., Stouffer, R. J., and Taylor, K. E.: Overview of the Coupled Model Intercomparison Project Phase 6 (CMIP6) experimental design and organization, Geoscientific Model Development, 9, 1937–1958, https://doi.org/10.5194/gmd-9-1937-2016, 2016.

Fischer, E. M. and Knutti, R.: Anthropogenic contribution to global occurrence of heavy-precipitation and high-temperature extremes, Nat. Clim. Chang., 5, 560–564, 2015.

Fischer, E. M., Beyerle, U., Schleussner, C. F., King, A. D., and Knutti, R.: Biased Estimates of Changes in Climate Extremes From Prescribed SST Simulations, Geophysical Research Letters, 45, 8500–8509, https://doi.org/https://doi.org/10.1029/2018GL079176, 2018.

FMI: Ilmastonmuutoksen vaikutus näkyi ennätyslämpimässä maaliskuussa, https://www.ilmatieteenlaitos.fi/puheenvuoro/2FPo2MDWBmp2jFPdbEBqGw, 2026.

Gao, M. and Franzke, C. L. E.: Quantile Regression–Based Spatiotemporal Analysis of Extreme Temperature Change in China, Journal of Climate, 30, 9897 – 9914, https://doi.org/10.1175/JCLI-D-17-0356.1, 2017.

Gilford, D. M., Pershing, A., Strauss, B. H., Haustein, K., and Otto, F. E. L.: A multi-method framework for global real-time climate attribution, Advances in Statistical Climatology, Meteorology and Oceanography, 8, 135–154, https://doi.org/10.5194/ascmo-8-135-2022, 2022.

https://doi.org/10.5194/egusphere-2026-3721
Preprint. Discussion started: 22 July 2026

Gottschalk, P. G. and Dunn, J. R.: The five-parameter logistic: A characterization and comparison with the four-parameter logistic, Analytical Biochemistry, 343, 54–65, https://doi.org/https://doi.org/10.1016/j.ab.2005.04.035, 2005.

Haugen, M. A., Stein, M. L., Moyer, E. J., and Sriver, R. L.: Estimating Changes in Temperature Distributions in a Large Ensemble of Climate Simulations Using Quantile Regression, Journal of Climate, 31, 8573 – 8588, https://doi.org/10.1175/JCLI-D-17-0782.1, 2018.

Hersbach, H., Bell, B., Berrisford, P., Hirahara, S., Horányi, A., Muñoz-Sabater, J., Nicolas, J., Peubey, C., Radu, R., Schepers, D., Simmons, A., Soci, C., Abdalla, S., Abellan, X., Balsamo, G., Bechtold, P., Biavati, G., Bidlot, J.-R., Bonavita, M., ..., and Thépaut, J.-N.: The ERA5 Global Reanalysis, Quarterly Journal of the Royal Meteorological Society, 146, 1999–2049, https://doi.org/10.1002/qj.3803, 2020.

Ionita, M. and Nagavciuc, V.: 2024: The year with too much summer in the eastern part of Europe, Weather, 80, 288–295, https://doi.org/https://doi.org/10.1002/wea.7696, 2025.

Jacob, D., Petersen, J., Eggert, B., Alias, A., Christensen, O. B., Bouwer, L. M., Braun, A., Colette, A., Déqué, M., Georgievski, G., Georgopoulou, E., Gobiet, A., Menut, L., Nikulin, G., Haensler, A., Hempelmann, N., Jones, C., Keuler, K., Kovats, S., Kröner, N., Kotlarski, S., Kriegsmann, A., Martin, E., van Meijgaard, E., Moseley, C., Pfeifer, S., Preuschmann, S., Radermacher, C., Radtke, K., Rechid, D., Rounsevell, M., Samuelsson, P., Somot, S., Soussana, J.-F., Teichmann, C., Valentini, R., Vautard, R., Weber, B., and Yiou, P.: EURO-CORDEX: New High-Resolution Climate Change Projections for European Impact Research, Regional Environmental Change, 14, 563–578, https://doi.org/10.1007/s10113-013-0499-2, 2014.

Joelsson, L. M. T., Engström, E., and Kjellström, E.: Homogenization of Swedish mean monthly temperature series 1860–2021, International Journal of Climatology, 43, 1079–1093, https://doi.org/https://doi.org/10.1002/joc.7881, 2023.

Kivinen, S., Rasmus, S., Jylhä, K., and Laapas, M.: Long-Term Climate Trends and Extreme Events in Northern Fennoscandia (1914–2013), Climate, 5, https://doi.org/10.3390/cli5010016, 2017.

Koenker, R. and Hallock, K. F.: Quantile Regression, Journal of Economic Perspectives, 15, 143–156, https://doi.org/10.1257/jep.15.4.143, 2001.

Koenker, R. W. and Bassett, G.: Regression quantiles, Econometrica, 46, 33–50, 1978.

Leach, N. J., Roberts, C. D., Aengenheyster, M., Heathcote, D., Mitchell, D. M., Thompson, V., Palmer, T., Weisheimer, A., and Allen, M. R.: Heatwave attribution based on reliable operational weather forecasts, Nat. Commun., 15, 4530, 2024.

Liao, J. J. Z. and Liu, R.: Re-parameterization of five-parameter logistic function, Journal of Chemometrics, 23, 248–253, https://doi.org/https://doi.org/10.1002/cem.1218, 2009.

Lorenz, E. N.: Deterministic Nonperiodic Flow, Journal of Atmospheric Sciences, 20, 130 – 141, https://doi.org/10.1175/1520-0469(1963)020<0130:DNF>2.0.CO;2, 1963.

Maibach, E., Cullen, H., Placky, B., Witte, J., and Gandy, J.: Improving public understanding of climate change by supporting weathercasters, Nat. Clim. Chang., 12, 694–695, 2022.

Mikkonen, S., Laine, M., Mäkelä, H. M., Gregow, H., Tuomenvirta, H., Lahtinen, M., and Laaksonen, A.: Trends in the Average Temperature in Finland, 1847–2013, Stochastic Environmental Research and Risk Assessment, 29, 1521–1529, https://doi.org/10.1007/s00477-014-0992-2, 2015.

Morice, C. P., Kennedy, J. J., Rayner, N. A., Winn, J. P., Hogan, E., Killick, R. E., Dunn, R. J. H., Osborn, T. J., Jones, P. D., and Simpson, I. R.: An Updated Assessment of Near-Surface Temperature Change From 1850: The HadCRUT5 Data Set, Journal of Geophysical Research: Atmospheres, 126, e2019JD032 361, https://doi.org/https://doi.org/10.1029/2019JD032361, e2019JD032361 2019JD032361, 2021.

Nature Climate Change: Advances in attribution, Nature Climate Change, 14, 1108–1108, 2024.

Otto, F. E.: Attribution of Weather and Climate Events, Annual Review of Environment and Resources, 42, 627–646, https://doi.org/https://doi.org/10.1146/annurev-environ-102016-060847, 2017.

Otto, F. E. L., Kew, S., Philip, S., Stott, P., and Oldenborgh, G. J. V.: How to Provide Useful Attribution Statements: Lessons Learned from Operationalizing Event Attribution in Europe, Bulletin of the American Meteorological Society, 103, S21 – S25, https://doi.org/10.1175/BAMS-D-21-0267.1, 2022.

Perkins, S. E., Alexander, L. V., and Nairn, J. R.: Increasing frequency, intensity and duration of observed global heatwaves and warm spells, Geophysical Research Letters, 39, https://doi.org/https://doi.org/10.1029/2012GL053361, 2012.

Philip, S., Kew, S., van Oldenborgh, G. J., Otto, F., Vautard, R., van der Wiel, K., King, A., Lott, F., Arrighi, J., Singh, R., and van Aalst, M.: A protocol for probabilistic extreme event attribution analyses, Advances in Statistical Climatology, Meteorology and Oceanography, 6, 177–203, https://doi.org/10.5194/ascmo-6-177-2020, 2020.

Philip, S. Y., Kew, S. F., van Oldenborgh, G. J., Anslow, F. S., Seneviratne, S. I., Vautard, R., Coumou, D., Ebi, K. L., Arrighi, J., Singh, R., van Aalst, M., Pereira Marghidan, C., Wehner, M., Yang, W., Li, S., Schumacher, D. L., Hauser, M., Bonnet, R., Luu, L. N., Lehner, F., Gillett, N., Tradowsky, J. S., Vecchi, G. A., Rodell, C., Stull, R. B., Howard, R., and Otto, F. E. L.: Rapid attribution analysis of the extraordinary heat wave on the Pacific coast of the US and Canada in June 2021, Earth System Dynamics, 13, 1689–1713, https://doi.org/10.5194/esd-13-1689-2022, 2022.

Poppick, A. and McKinnon, K. A.: Observation-Based Simulations of Humidity and Temperature Using Quantile Regression, Journal of Climate, 33, 10 691 – 10 706, https://doi.org/10.1175/JCLI-D-20-0403.1, 2020.

Rahmstorf, S. and Coumou, D.: Increase of extreme events in a warming world, Proceedings of the National Academy of Sciences, 108, 17 905–17 909, https://doi.org/10.1073/pnas.1101766108, 2011.

Räisänen, J., Rantanen, M., and Toropainen, A.: Estimating Present Temperature Climate in a Warming World: Probabilistic Verification of a Model-Based Approach for Years 2008–2023, Research Square, https://doi.org/10.21203/rs.3.rs-5602233/v1, preprint, under review, 2025.

Rantanen, M., Räisänen, J., and Merikanto, J.: A method for estimating the effect of climate change on monthly mean temperatures: September 2023 and other recent record-warm months in Helsinki, Finland, Atmospheric Science Letters, 25, e1216, https://doi.org/https://doi.org/10.1002/asl.1216, 2024.

Rantanen, M., Helama, S., Räisänen, J., and Gregow, H.: Summer 2024 in northern Fennoscandia was very likely the warmest in 2000 years, npj Climate and Atmospheric Science, 8, https://doi.org/10.1038/s41612-025-01046-4, 2025.

Ricketts, J. H. and Head, G. A.: A five-parameter logistic equation for investigating asymmetry of curvature in baroreflex studies, American Journal of Physiology-Regulatory, Integrative and Comparative Physiology, 277, R441–R454, https://doi.org/10.1152/ajpregu.1999.277.2.R441, 1999.

Ruosteenoja, K. and Räisänen, J.: Evolution of observed and modelled temperatures in Finland in 1901–2018 and potential dynamical reasons for the differences, International Journal of Climatology, 41, 3374–3390, https://doi.org/https://doi.org/10.1002/joc.7024, 2021.

Räisänen, J.: Effect of atmospheric circulation on recent temperature changes in Finland, Climate Dynamics, 53, 5675–5687, https://doi.org/10.1007/s00382-019-04890-2, 2019.

Räisänen, J. and Ruokolainen, L.: Estimating present climate in a warming world: a model-based approach, Climate Dynamics, 31, https://doi.org/10.1007/s00382-007-0361-7, 2008a.

Räisänen, J. and Ruokolainen, L.: Ongoing Global Warming and Local Warm Extremes: a Case Study of Winter 2006-2007 in Helsinki, Finland, Geophysica, 44, 2008b.

https://doi.org/10.5194/egusphere-2026-3721
Preprint. Discussion started: 22 July 2026

Seneviratne, S. I., Zhang, X., Adnan, M., Badi, W., Dereczynski, C., Di Luca, A., Ghosh, S., Iskander, I., Kossin, J., Lewis, S., Otto, F., Pinto, I., Satoh, M., Vicente-Serrano, S. M., Wehner, M., and Zhou, B.: Weather and Climate Extreme Events in a Changing Climate (Chapter 11), in: IPCC 2021: Climate Change 2021: The Physical Science Basis. Contribution of Working Group I to the Sixth Assessment Report of the Intergovernmental Panel on Climate Change, edited by Masson-Delmotte, V., Zhai, P., Pirani, A., Connors, S., Péan, C., Berger, S., Caud, N., Chen, Y., Goldfarb, L., Gomis, M., Huang, M., Leitzell, K., Lonnoy, E., Matthews, J., Maycock, T., Waterfield, T., Yelekçi, K., Yu, R., and Zhu, B., pp. 1513–1766, Cambridge University Press, Cambridge, United Kingdom and New York, NY, USA, https://doi.org/10.1017/9781009157896.013, 2021.

Skålevåg, A.: Attribusjon av årsmiddeltemperaturer i 2025 ved utvalgte norske stasjoner, MET Report 01/2026, Norwegian Meteorological Institute (MET Norway), https://www.met.no/publikasjoner/met-report/_/attachment/inline/24695108-be85-47f5-a377-7be5246d8ba0:af0eb37dd5eba440ca3f856973554ff04b033e45/Met-report-01-2026.pdf, 2026.

Stott, P. A. and Christidis, N.: Operational attribution of weather and climate extremes: what next?, Environmental Research: Climate, 2, 013 001, https://doi.org/10.1088/2752-5295/acb078, 2023.

Sulikowska, A. and Wypych, A.: Seasonal Variability of Trends in Regional Hot and Warm Temperature Extremes in Europe, Atmosphere, 12, https://doi.org/10.3390/atmos12050612, 2021.

Toropainen, A., Rantanen, M., and Räisänen, J.: The code and input dataset for ATDT (Attribution tool for Daily-to-monthly Temperatures), https://doi.org/10.5281/zenodo.20742664, 2026.

Uhe, P., Otto, F. E. L., Haustein, K., van Oldenborgh, G. J., King, A. D., Wallom, D. C. H., Allen, M. R., and Cullen, H.: Comparison of methods: Attributing the 2014 record European temperatures to human influences, Geophysical Research Letters, 43, 8685–8693, https://doi.org/https://doi.org/10.1002/2016GL069568, 2016.

van Oldenborgh, G. J., van der Wiel, K., Kew, S., Philip, S., Otto, F., Vautard, R., King, A., Lott, F., Arrighi, J., Singh, R., and van Aalst, M.: Pathways and pitfalls in extreme event attribution, Climatic change, 166, https://doi.org/10.1007/s10584-021-03071-7, publisher Copyright: © 2021, The Author(s)., 2021.

Wasko, C. and Sharma, A.: Quantile regression for investigating scaling of extreme precipitation with temperature, Water Resources Research, 50, 3608–3614, https://doi.org/https://doi.org/10.1002/2013WR015194, 2014.

Wells, C. D., Jackson, L. S., Maycock, A. C., and Forster, P. M.: Understanding pattern scaling errors across a range of emissions pathways, Earth System Dynamics, 14, 817–834, https://doi.org/10.5194/esd-14-817-2023, 2023.

World Weather Attribution: World Weather Attribution – Exploring the contribution of climate change to extreme weather events, https://www.worldweatherattribution.org/, accessed: 2026-06-02, 2026.

Zhang, Y., Ayyub, B. M., Fung, J. F., and Labe, Z. M.: Incorporating extreme event attribution into climate change adaptation for civil infrastructure: Methods, benefits, and research needs, Resilient Cities and Structures, 3, 103–113, https://doi.org/https://doi.org/10.1016/j.rcns.2024.03.002, 2024.